Stability analysis of highly variable soils by elasto-plastic finite elements

D.V. Griffiths

Colorado School of Mines, Golden, Colorado, U.S.A.

Abstract. Geotechnical analyses involving bearing capacity, excavation and slope stability of highly variable soils have been performed using elasto-plastic finite elements. The finite element analyses are validated against well-known solutions where possible, before being applied to more complicated problems in which the classical approaches are at best inconvenient, and at worst may lead to misleading results. The types of heterogeneity considered in this work include simple layering due to stratification, water table effects, voids due to excavation and variability based on a statistical description of the material properties. In the statistical approach, the results lead to a probabilistic interpretation of design parameters that have traditionally been dealt with using "average" soil properies in conjunction with a "Factor of Safety".

1 Slope Stability Analysis by Finite Elements

The majority of slope stability analyses performed in practice still use traditional limit equilibrium approaches involving methods of slices that have remained essentially unchanged for decades. This was not the outcome envisaged when Whitman and Bailey (1967) set criteria for the then emerging methods to become readily accessible to all engineers.

The finite element method represents a powerful alternative approach for slope stability analysis which is accurate, versatile and requires fewer *a priori* assumptions, especially regarding the failure mechanism. Slope failure in the finite element model occurs "naturally" through the zones in which the shear strength of the soil is insufficient to resist the shear stresses. This section, which is based on a paper by Griffiths and Lane (1999), describes several examples of finite element slope stability analysis with comparison against other solution methods, including the influence of a layering and a free surface on slope and dam stability. Graphical output is included to illustrate deformations and mechanisms of failure.

It is argued that the finite element method of slope stability analysis is a more powerful alternative to traditional limit equilibrium methods and its widespread use should now be standard in geotechnical practice.

1.1 Introduction

Elasto-plastic analysis of geotechnical problems using the finite element (FE) method has been widely accepted in the research arena for many years, however its routine use in

geotechnical practice for slope stability analysis still remains limited. The reason for this lack of acceptance is not entirely clear, however advocates of finite element techniques in academe must take some responsibility. Practicing engineers are often sceptical of the need for such complexity especially in view of the poor quality of soil property data often available from routine site investigations. Although this scepticism is often warranted, there *are* certain types of geotechnical problem for which the finite element approach offers real benefits. The challenge for an experienced engineer is to know which kind of problem would benefit from a finite element treatment and which would not.

In general, linear problems such as the prediction of settlements and deformations, the calculation of flow quantities due to steady seepage or the study of transient effects due to consolidation are all highly amenable to solution by finite elements. Traditional approaches involving charts, tables or graphical methods will often be adequate for routine problems but the finite element approach may be valuable if awkward geometries or material variations are encountered which are not covered by traditional chart solutions.

The use of nonlinear analysis in routine geotechnical practice is harder to justify because there is usually a significant increase in complexity which is more likely to require the help of a modelling specialist. Nonlinear analyses are inherently iterative in nature, because the material properties and/or the geometry of the problem are themselves a function of the "solution". Objections to nonlinear analysis on the grounds that they require excessive computational power however have been largely overtaken by developments in, and falling costs of, computer hardware. A desktop computer with a standard processor is now capable of performing nonlinear analyses such as those described in this report in a reasonable time span - minutes rather than hours or days.

Slope stability represents an area of geotechnical analysis in which a nonlinear finite element approach offers real benefits over existing methods. As this report will show, slope stability analysis by elasto-plastic finite elements is accurate, robust and simple enough for routine use by practicing engineers. Perception of the finite element method as complex and potentially misleading is unwarranted and ignores the real possibility that misleading results can be obtained with conventional "slip circle" approaches. The graphical capabilities of FE programs also allow better understanding of the mechanisms of failure, simplifying the output from reams of paper to managable graphs and plots of displacements.

1.2 Traditional Methods of Slope Stability Analysis

Most textbooks on soil mechanics or geotechnical engineering will include reference to several alternative methods of slope stability analysis. In a survey of equilibrium methods of slope stability analysis reported in Duncan's 1996 'State of the Art' review, the characteristics of a large number of methods were summarised including the Ordinary Method of Slices (Fellenius 1936), Bishop's Modified Method (1955), Force Equilibrium Methods (e.g. Lowe and Karafiath 1960), Janbu's Generalised Procedure of Slices (1968), Morgenstern and Price's Method (1965) and Spencer's Method (1967).

Although there seems to be some consensus that Spencer's Method is one of the most reliable, textbooks continue to describe the others in some detail and the wide selection of available methods is at best confusing to the potential user. For example, the

2

controversy was recently revisited by Lambe and Silva (1995) who maintained that the Ordinary Method of Slices had an undeservedly bad reputation.

A difficulty with *all* the equilibrium methods is that they are based on the assumption that the failing soil mass can be divided into slices. This in turn necessitates further assumptions relating to side force directions between slices, with consequent implications for equilibrium. The side force assumption is one of the main characteristics distinguishing one limit equilibrium method from another, yet the concept of side forces is entirely artificial.

1.3   Finite Element Methods for Slope Stability Analysis

Duncan's review of finite element analysis of slopes concentrated mainly on deformation rather than stability analysis of slopes, however, attention was drawn to some important early papers in which elasto-plastic soil models were used to assess stability. Smith and Hobbs (1974) reported results of $\phi_u = 0$ slopes and obtained reasonable agreement with Taylor's (1937) charts. Zienkiewicz *et al* (1975) considered a c', ϕ' slope and obtained good agreement with slip circle solutions. Griffiths (1980) extended this work to show reliable slope stability results over a wide range of soil properties and geometries as compared with charts of Bishop and Morgenstern (1960). Subsequent use of the finite element method in slope stability analysis has added further confidence in the method, (e.g. Griffiths 1989, Potts *et al* 1990, Matsui and San 1992). Duncan mentions the potential for improved graphical results and reporting utilising FE but cautions against artificial accuracy being assumed when the input parameters themselves are so variable.

Wong (1984) gives a useful summary of potential sources of error in the finite element modelling of slope stability, although recent results, including those presented in this paper, indicate that better accuracy is now possible.

Advantages of the Finite Element Method. The advantages of a finite element approach to slope stability analysis over traditional limit equilibrium methods can be summarised as follows:

1. No assumption needs to be made in advance about the shape or location of the failure surface. Failure occurs "naturally" through the zones within the soil mass in which the soil shear strength is unable to resist the applied shear stresses.
2. Since there is no concept of slices in the finite element approach there is no need for assumptions about slice side forces. The finite element method preserves global equilibrium until "failure" is reached.
3. If realistic soil compressibility data is available, the finite element solutions will give information about deformations at working stress levels.
4. The finite element method is able to monitor progressive failure up to and including overall shear failure.

Brief Description of the Finite Element Model. The programs used in this paper are based closely on Program 6.2 in the text by Smith and Griffiths (1998)–the main

difference being the ability to model more general geometries and soil property variations including variable water levels and pore pressures. Further graphical output capabilities have also been added. The programs are for 2-d plane strain analysis of elastic-perfectly plastic soils with a Mohr-Coulomb failure criterion utilising 8-node quadrilateral elements with reduced integration (4 Gauss-points per element) in the gravity loads generation, the stiffness matrix generation and the stress redistribution phases of the algorithm. The soil is initially assumed to be elastic and the model generates normal and shear stresses at all Gauss-points within the mesh. These stresses are then compared with the Mohr-Coulomb failure criterion. If the stresses at a particular Gauss-point lie within the Mohr-Coulomb failure envelope then that location is assumed to remain elastic. If the stresses lie on or outside the failure envelope, then that location is assumed to be yielding. Yielding stresses are redistributed throughout the mesh utilising the visco-plastic algorithm (Perzyna 1966, Zienkiewicz and Cormeau 1974). Overall shear failure occurs when a sufficient number of Gauss-points have yielded to allow a mechanism to develop.

The analyses presented in this paper do not attempt to model tension cracks. Although "no-tension" criteria can be incorporated into elasto-plastic finite element analyses (see e.g. Naylor and Pande 1981), this additional constraint on stress levels complicates the algorithm, and in addition, there is still some debate as to how "tension" should properly be defined. Further research in this area is warranted,

Soil Model. The soil model used in this study consists of six parameters as shown in Table 1.1

<div align="center">

Table 1.1. Six parameter soil model

ϕ'	Friction angle
c'	Cohesion
ψ	Dilation angle
E'	Young's modulus
ν'	Poisson's ratio
γ	Unit weight

</div>

The dilation angle ψ affects the volume change of the soil during yielding. It is well known that the actual volume change exhibited by a soil during yielding is quite variable. For example a medium dense material during shearing might initially exhibit some volume decrease ($\psi < 0$) followed by a dilative phase ($\psi > 0$), leading eventually to yield under constant volume conditions ($\psi = 0$). Clearly this type of detailed volumetric modelling is beyond the scope of the elastic-perfectly plastic models used in this study where a constant dilation angle is implied.

The question then arises as to what value of ψ to use. If $\psi = \phi'$ then the plasticity flow rule is "associated" and direct comparisons with theorems from classical plasticity can be made. It is also the case that when the flow rule is associated, the stress and velocity characteristics coincide, thus closer agreement can be expected between failure

mechanisms predicted by finite elements and critical failure surfaces generated by limit equilibrium methods.

In spite of these potential advantages of using an associated flow rule, it is also well known that associated flow rules with frictional soil models predict far greater dilation than is ever observed in reality. This in turn leads to increased failure load prediciton, especially in "confined" problems such as bearing capacity (Griffiths 1982). This shortcoming has led some of the more successful constitutive soil models to incorporate non-associated plasticity (e.g. Molenkamp 1981, Griffiths *et al* 1982, Hicks and Boughrarou 1998).

Slope stability analysis is relatively unconfined, thus the choice of dilation angle is less important. As the main objective of the current study is the accurate prediction of slope factors of safety, a compromise value of $\psi = 0$, corresponding to a non-associated flow rule with zero volume change during yield, has been used throughout this report. It will be shown that this value of ψ enables the model to give reliable factors of safety and a reasonable indication of the location and shape of the potential failure surfaces.

The parameters c' and ϕ' refer to the effective cohesion and friction angle of the soil. Although a number of failure criteria have been suggested for modelling the strength of soil (see e.g. Griffiths 1990) , Mohr-Coulomb's criterion remains the one most widely used in geotechnical practice and has been used throughout this paper. In terms of principal stresses and assuming a compression-negative sign convention, the criterion can be written as follows:

$$F = \frac{\sigma'_1 + \sigma'_3}{2} \sin \phi' - \frac{\sigma'_1 - \sigma'_3}{2} - c' \cos \phi' \tag{1}$$

where σ'_1 and σ'_3 are the major and minor principal effective stresses.

The failure function F can be interpreted as follows:

$F < 0$ stresses inside failure envelope (elastic)
$F = 0$ stresses on failure envelope (yielding)
$F > 0$ stresses outside failure envelope (yielding and must be redistributed)

The elastic parameters E' and ν' refer to Young's modulus and Poisson's ratio of the soil. If a value of Poisson's ratio is assumed (typical drained values lie in the range $0.2 < \nu' < 0.3$), the value of Young's modulus can be related to the compressibility of the soil as measured in a 1-d oedometer (see e.g. Lambe and Whitman 1969) ,

$$E' = \frac{(1 + \nu')(1 - 2\nu')}{m_v(1 - \nu')} \tag{2}$$

where m_v is the coefficient of volume compressibility.

Although the actual values given to the elastic parameters have a profound influence on the computed deformations prior to failure, they have little influence on the predicted factor of safety in slope stability analysis. Thus, in the absence of meaningful data for E' and ν', they can be given nominal values (e.g. $E' = 10^5$ kN/m^2 and $\nu' = 0.3$).

The total unit weight γ assigned to the soil is proportional to the nodal self-weight loads generated by gravity and will be discussed further in the next section.

In summary, the most important parameters in a finite element slope stability analysis are the same as they would be in a traditional limit equilibrium approach, namely the total unit weight γ, the shear strength parameters c' and ϕ' and the geometry of the problem.

Gravity Loading. The forces generated by the self weight of the soil are computed using a standard gravity "turn-on" procedure involving integrals over each element of the form:

$$\mathbf{p}^{(e)} = \gamma \int_{V^e} \mathbf{N}^T \, dV^e \tag{3}$$

where $\mathbf{N}$ are the shape functions of the element and the superscript e refers to the element number. This integral evaluates the volume of each element, multiplies by the total unit weight of the soil and distributes the net vertical force consistently to all the nodes. These element forces are assembled into a global gravity force vector that is applied to the finite element mesh in order to generate the initial stress state of the problem.

The present work applies gravity in a single increment to an initially stress-free slope. Others have shown that under elastic conditions, sequential loading in the form of incremental gravity application or embanking, affects deformations but not stresses (see e.g. Clough and Woodward 1967). In nonlinear analyses, it is recognised that the stress paths followed due to sequential excavation may be quite different to those followed under a gravity "turn-on" procedure, however the factor of safety appears unaffected when using simple elasto-plastic models (see.e.g Borja *et al* 1989, Smith and Griffiths 1998).

In comparing results with limit equilibrium solutions which generally take no account of loading sequence, experience has shown that the predicted factor of safety is insensitive to the form of gravity application when using elastic-perfectly plastic Mohr-Coulomb models. An example of this insensitivity is demonstrated later in the report.

The factor of safety may be sensitive to loading sequence when implementing more complex constitutive laws, such as those that attempt to reproduce volumetric changes accurately in an undrained or partially drained environment. For example, Hicks and Wong (1988) showed that the effective stress path could have a big influence on the factor of safety of an undrained slope.

Determination of the Factor of Safety The Factor of Safety (FOS) of a soil slope is defined here as the factor by which the original shear strength parameters must be divided in order to bring the slope to the point of failure.[1] The factored shear strength parameters c'_f and ϕ'_f, are therefore given by:

$$c'_f = c'/SRF \tag{4}$$

---

[1] This definition of the factor of safety is exactly the same as that used in traditional limit equilibrium methods, namely the ratio of restoring to driving moments.

$$\phi_f^{'} = \arctan(\frac{\tan \phi^{'}}{SRF}) \tag{5}$$

where SRF is a "Strength Reduction Factor". This method is referred to as the "shear strength reduction technique" (e.g. Matsui and San 1992) and allows for the interesting option of applying different strength reduction factors to the $c^{'}$ and $\tan \phi^{'}$ terms. In this paper however, the same factor is always applied to both terms. To find the "true" factor of safety FOS, it is necessary to initiate a systematic search for the value of SRF that will just cause the slope to fail. When this value has been found, $FOS = SRF$.

Definition of Failure. There are several possible definitions of failure e.g. some test of bulging of the slope profile (Snitbhan and Chen 1976); limiting of the shear stresses on the potential failure surface (Duncan and Dunlop 1969) or nonconvergence of the solution (Zienkiewicz and Taylor 1989). These are discussed in Abramson *et al* (1995) from the original paper by Wong (1984) but without resolution. In the examples studied here the non-convergence option is taken as being a suitable indicator of failure.

When the algorithm cannot converge within a user-specified maximum number of iterations, the implication is that no stress distribution can be found that is simultaneously able to satisfy both the Mohr-Coulomb failure criterion and global equilibrium. If the algorithm is unable to satisfy these criteria "failure" is said to have occurred. Slope failure and numerical non-convergence occur simultaneously, and are accompanied by a dramatic increase in the nodal displacements within the mesh. Most of the results shown in this section used an iteration ceiling of 1000 and present results in the form of a graph of SRF vs. $E^{'}\delta_{max}/\gamma H^2$ (a dimensionless displacement), where δ_{max} is the maximum nodal displacement at convergence and H is the height of the slope. This graph may be used alongside the displaced mesh and vector plots to indicate both the factor of safety and the nature of the failure mechanism.

1.4 Slope Stability Examples and Validation

Several examples of finite element slope stability analysis are now presented with validation against traditional stability analyses where possible. Initial consideration will be given to slopes containing no pore pressures in which total and effective stresses are equal. This is followed by examples of layered slopes. Finally, submerged and partially submerged slopes are considered in which pore pressures are taken into account.

Example 1: Homogeneous slope with no foundation layer (D=1). The homogeneous slope shown in Figure 1 has the following soil properties:

$$\begin{aligned} \phi^{'} &= 20^o \\ c^{'}/\gamma H &= 0.05 \end{aligned}$$

The slope is inclined at an angle of 26.57^o (2:1) to the horizontal and the boundary conditions are given as vertical rollers on the left boundary and full fixity at the base.
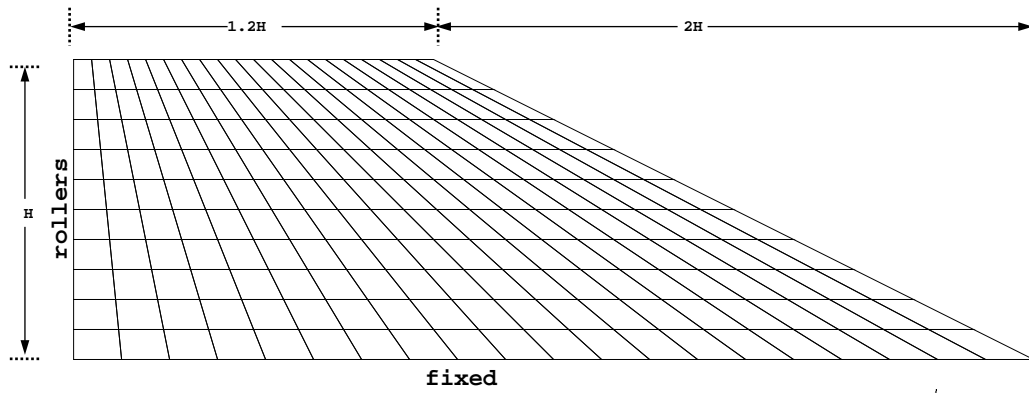
Figure 1. Example 1: Mesh for a homogeneous slope with a slope angle of 26.57^o (2:1), $\phi' = 20^o$, $c'/\gamma H = 0.05$
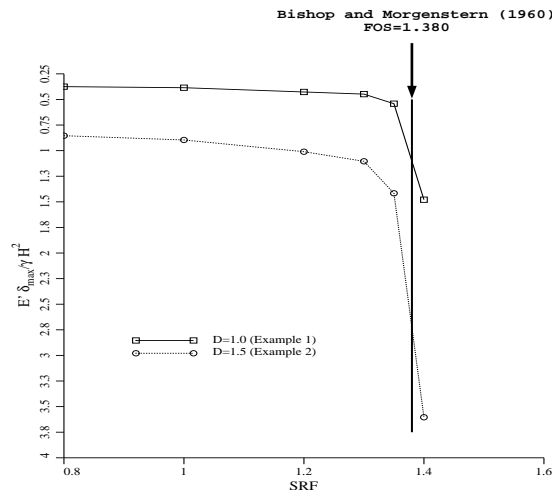

Figure 2. Examples 1 and 2: SRF vs. Dimensionless displacement. The rapid increase in displacement and the lack of convergence when $FOS = 1.4$ indicates slope failure.
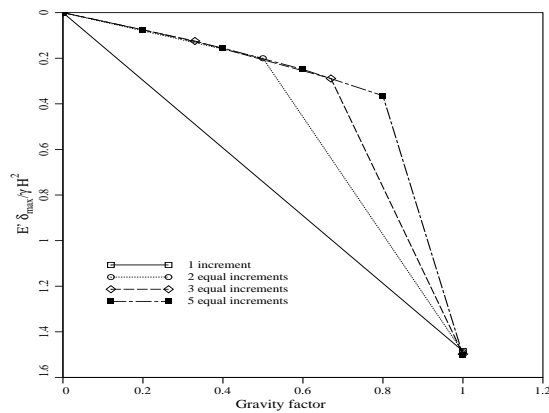

Figure 3. Influence of gravity increment size on maximum displacement at failure (FOS=1.4) from Example 1.

Gravity loads were applied to the mesh and the strength reduction factor (SRF) gradually increased until convergence could not be achieved within the iteration limit as shown in Table 1.2.

Table 1.2. Results from Example 1

SRF	$E^{'}\delta_{max}/\gamma H^2$	Iterations
0.80	0.379	2
1.00	0.381	10
1.20	0.422	20
1.30	0.453	41
1.35	0.544	792
1.40	1.476	1000

The table indicates that six trial strength reduction factors were attempted ranging from 0.8 to 1.4. Each value represented a completely independent analysis in which the soil strength parameters were scaled by SRF as indicated in equations 4 and 5. Some efficiencies are possible in that the gravity loads and global stiffness matrix are the same in each analysis and are therefore generated once only.

The "Iterations" column indicates the number of iterations for convergence corresponding to each SRF value. The algorithm has to work harder to achieve convergence as the "true" FOS is approached. When $SRF = FOS = 1.4$, there is a sudden increase in the dimensionless displacement $E^{'}\delta_{max}/\gamma H^2$, and the algorithm is unable to converge within the iteration limit. Figure 2 shows a plot of the data from Table 1.2 and indicates close agreement between the finite element result and the factor of safety given for the same problem by the charts of Bishop and Morgenstern (1960).

Figure 3 shows the influence of gravity loading increment size on displacements in Example 1. With a "failure" strength reduction factor of $SRF = 1.4$ applied to the soil properties, the four graphs correspond to the maximum displacement obtained when gravity was applied in a single increment as compared with that obtained with 2, 3 or 5 equal increments. The figure demonstrates that the displacement obtained with full gravity loading is barely affected by the increment size.

Figures 4a and 4b give the nodal displacement vectors and the deformed mesh corresponding to the unconverged situation with $SRF = FOS = 1.4$. The deformed mesh corresponding to this unconverged solution gives a rather diffuse indication of the failure mechanism. This is due to the relatively crude finite element mesh which must remains continuous even at "failure". Continuum finite element analysis is unable to model gross discontinuities along potential failure surfaces although techniques have been described for enhancing the visualisation of the failure surfaces (see e.g. Griffiths and Kidger 1995). More advanced finite element methods for modelling shear bands in conjunction with adaptive mesh refinement techniques have been described by Loret and Prevost (1991) and Zienkiewicz et al (1995).

9

(a)

(b)
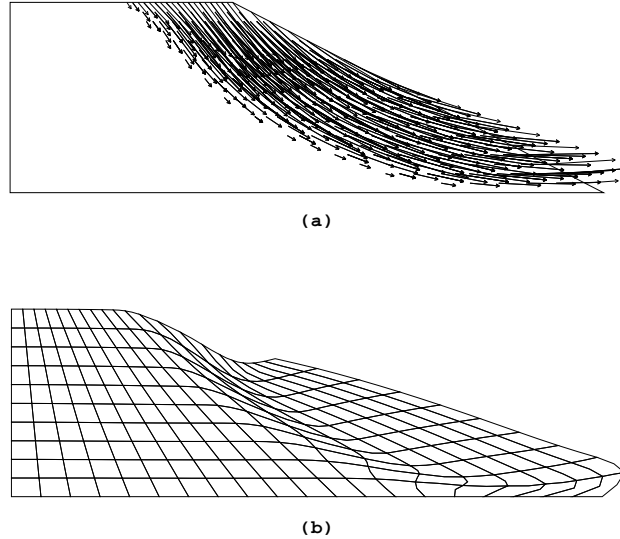
Figure 4. Example 1: Deformed mesh plots corresponding to the unconverged solution with FOS=1.4. (a) Nodal displacement vectors, (b) Deformed mesh.
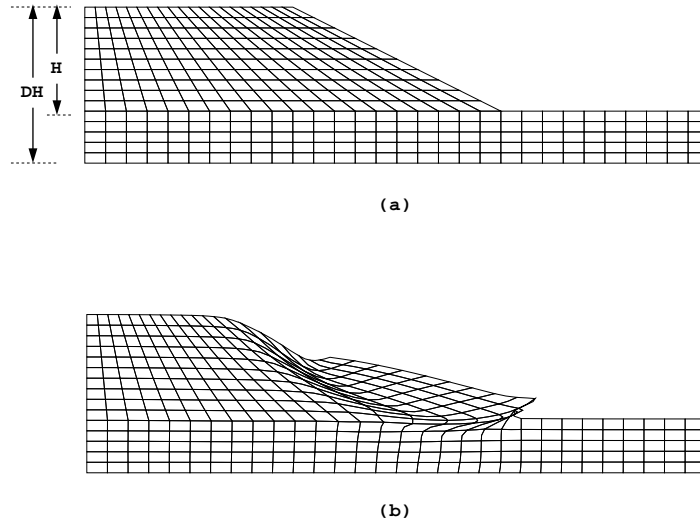
Example 2: Homogeneous slope with a foundation layer (D=1.5). In this example, a foundation layer of thickness $H/2$ has been added to the base of the slope of Example 1 with all other properties and geometry remaining the same.

The initial mesh and the deformed mesh at failure are shown in Figures 5a and 5b respectively. It is clear from Figure 5b, that a mechanism of the "toe failure" type has been obtained. Figure 2 indicates that the critical factor of safety is essentially unchanged from Example 1 at $FOS = 1.4$ although the displacements are increased due to the greater volume of compressible soil.

This finite element result confirms that the addition of the foundation layer has *not* led to any perceptible change in the Factor of Safety of the slope. Bishop and Morgenstern (1960) give $FOS = 1.752$ as one possible solution for this example ($D = 1.5, c'/\gamma H = 0.05, \phi' = 20°$, 2:1 slope) although it is important to check the alternative solution corresponding to D=1.0 to verify which gives the lower FOS. The charts of Cousins (1978) essentially agree with the finite element result and indicate that with a foundation layer, the critical circular mechanism at its lowest point passes fractionally below the base of the slope and gives a slightly lower factor of safety than when there is no foundation layer present.

Solving this example using a proprietary slip circle program also found the possible "result" of $FOS = 1.7$ when a failure circle tangent to the base of the foundation was assumed. It was necessary to force the slip circle to pass through the toe to obtain the "correct" $FOS = 1.37$.

This example demonstrates one of the main advantages of finite element slope stability analysis over conventional methods. The FE approach requires no *a priori* assumption of the location or shape of the critical surface. Failure occurs "naturally" within the zones of the soil mass where the shear strength of the soil is insufficient to resist the shear stresses.

10

(a)

(b)

Figure 5. Example 2: Homogeneous slope with a foundation layer. Slope angle 26.57° (2:1), $\phi' = 20^\circ$, $c'/\gamma H = 0.05$, $D = 1.5$. (a) Undeformed mesh, (b) Mesh corresponding to unconverged solution with $FOS = 1.4$.

The use of a limit equilibrium methods at the very least, requires some experience and care on the part of the user in order to initiate appropriate search procedures which avoid the possibility of homing in on the wrong "critical" circle.

Example 3: An undrained clay slope failure with a thin weak layer. Figure 6 shows a slope on a foundation layer ($D = 2$) of undrained clay. The slope includes a thin layer of weaker material which initially runs parallel to the slope, then horizontally in the foundation and finally outcrops at an angle of 45° beyond the toe.
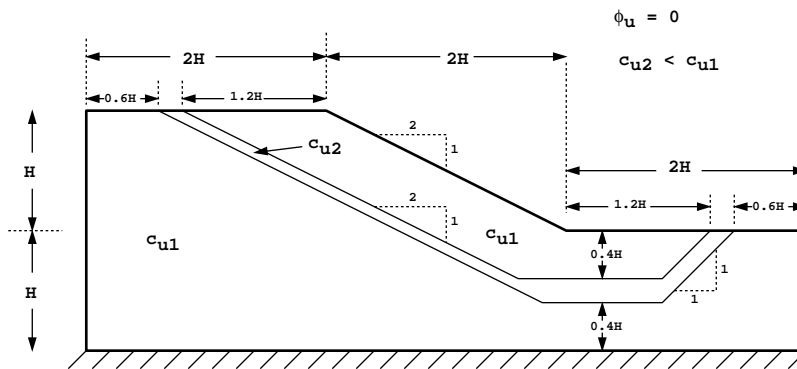
Figure 6. Example 3: Undrained clay slope with a foundation layer including a thin weak layer ($D = 2$, $c_{u1}/\gamma H = 0.25$)

11

Although this example may seem contrived, it is not unlike the situation of a thin, "slippery" liner within a landfill system. The factor of safety of the slope was estimated by finite element analysis for a range of values of the undrained shear strength of the thin layer (c_{u2}) while maintaining the strength of the surrounding soil at $c_{u1}/\gamma H = 0.25$.
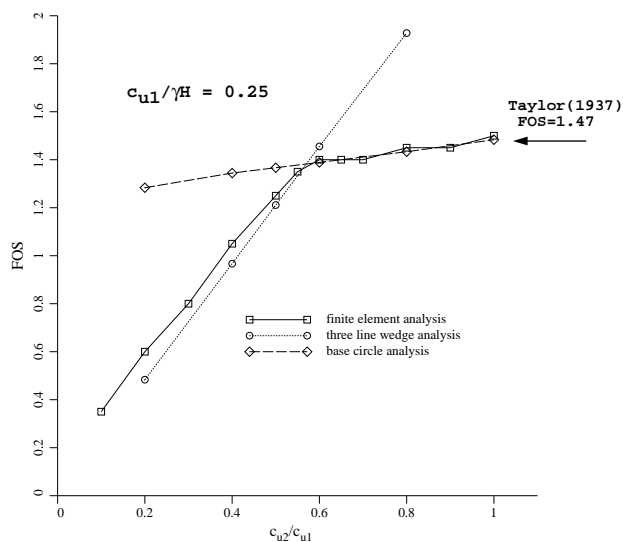

Figure 7. Example 3: Computed factor of safety (FOS) for different values of c_{u2}/c_{u1}.

The finite element results shown in Figure 7 give the computed factor of safety expressed to the nearest 0.05. For a homogeneous slope ($c_{u2}/c_{u1} = 1$), the computed factor of safety was close to the Taylor solution (Taylor 1937) of $FOS = 1.47$ and gave the expected circular base failure mechanism. As the strength of the thin layer was gradually reduced, a distinct change in the nature of the results was observed when $c_{u2}/c_{u1} \approx 0.6$.

Also shown on this figure are limit equilibrium solutions obtained using Janbu's method assuming both circular (base failure) and three line wedge mechanisms following the path of the weak layer. The discontinuity when $c_{u2}/c_{u1} \approx 0.6$ clearly represents the transition between the circular mechanism and the non-circular mechanism governed by the weak layer. For $c_{u2}/c_{u1} > 0.6$ the (circular) base failure mechanism governs the behaviour and the factor of safety is essentially unaffected by the strength of the weaker thin layer. For $c_{u2}/c_{u1} < 0.6$ the (non-circular) thin layer mechanism takes over and the factor of safety falls linearly.

This behaviour is explained more clearly in Figure 8 which shows the deformed mesh at failure for three different values of the ratio c_{u2}/c_{u1}. Figure 8a, corresponding to the homogeneous case ($c_{u2}/c_{u1} = 1$), indicates an essentially circular failure mechanism tangent to the firm base as predicted by Taylor. Figure 8c, in which the strength of the thin layer is only 20% of the surrounding soil ($c_{u2}/c_{u1} = 0.2$), indicates a highly concentrated non-circular mechanism closely following the path of the thin weak layer. Figure 8b, in which the strength of the thin layer is 60% of the surrounding soil ($c_{u2}/c_{u1} =$

12
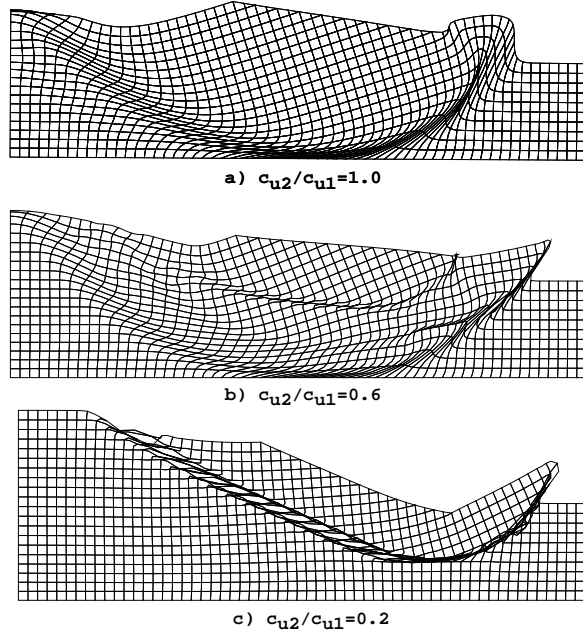
Figure 8. Example 3: Deformed meshes at failure corresponding to the unconverged solution for three different values of c_{u2}/c_{u1}.

0.6) indicates considerable complexity and ambiguity. At least two conflicting mechanisms are apparent. Firstly there is a base failure mechanism merging with the weak layer beyond the toe of the slope and secondly there is a mechanism running along the weak layer parallel to the slope and outcropping at the toe.

Without prior knowledge of the two alternative mechanisms, a traditional limit equilibrium search could overestimate the factor of safety. This is illustrated in Figure 7 where, for example, a circular mechanism with $c_{u2}/c_{u1} = 0.2$ would indicate $FOS = 1.3$ when the correct factor of safety is closer to 0.6.

Example 4: An undrained clay slope with a weak foundation layer. In this case, the same slope geometry and finite element mesh as in the previous example has been used but with a different type of inhomogeneity as shown in Figure 9. The shear strength of the slope material has been maintained at a constant value of $c_{u1}/\gamma H = 0.25$ while the shear strength of the foundation layer has been varied. The relative size of the two shear strengths has again been expressed as the ratio c_{u2}/c_{u1}. Figure 10 shows the

13

computed factor of safety for a range of c_{u2}/c_{u1} values together with classical solutions of Taylor for the two cases when $c_{u2} = c_{u1}$ and $c_{u2} \gg c_{u1}$.
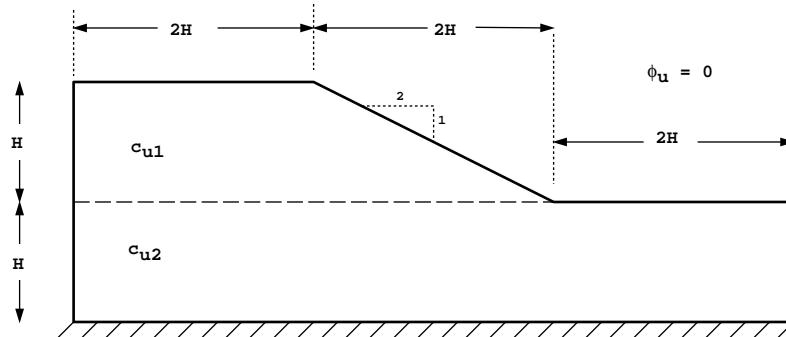
**Figure 9.** Example 4: Undrained clay slope with a weak foundation layer ($D = 2$, $c_{u1}/\gamma H = 0.25$)

There is clearly a change of behavior occurring at $c_{u2}/c_{u1} \approx 1.5$ as indicated by the flattening out of the curve. Also shown on this figure are limit equilibrium solutions for both toe and base circle mechanisms. The discontinuity corresponding to $c_{u2}/c_{u1} \approx 1.5$ obviously represents the transition between these two fundamental mechanisms.
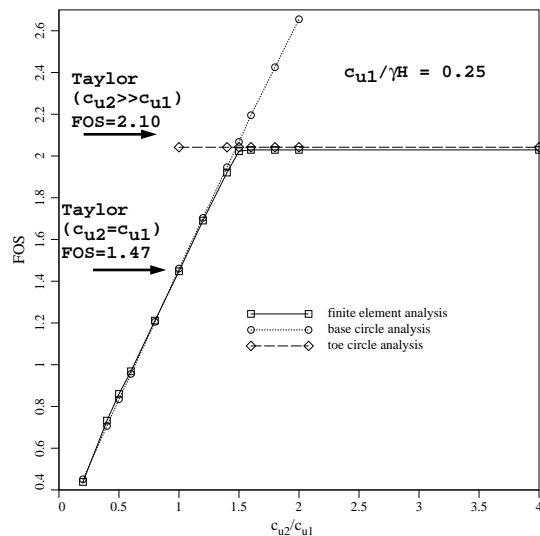
Figure 10. Example 4: Computed factor of safety (FOS) for different values of c_{u2}/c_{u1}.

This transition is clearly demonstrated by the finite element failure mechanisms shown in Figure 11. When $c_{u2} \ll c_{u1}$ (Figure 11a) a deep-seated base mechanism is observed,

14

whereas a shallow "toe" mechanism is seen when $c_{u2} \gg c_{u1}$ (Figure 11c). The result corresponding to the approximate transition point at $c_{u2} \approx 1.5c_{u1}$ (Figure 11b) shows an ambiguous situation in which both mechanisms are trying to form at the same time. It is interesting to note that the lower soil must be at least 50% stronger than the upper soil before the toe mechanism becomes the most critical. The slip circle program STABR (Duncan and Wong, 1985) when applied to this example with $c_{u2}/c_{u1} = 1.46$ gave identical Factors of Safety of 2.02 for circles tangent to the base of the slope and the base of the foundation.

a) $c_{u2}/c_{u1}=0.6$

b) $c_{u2}/c_{u1}=1.5$

c) $c_{u2}/c_{u1}=2.0$
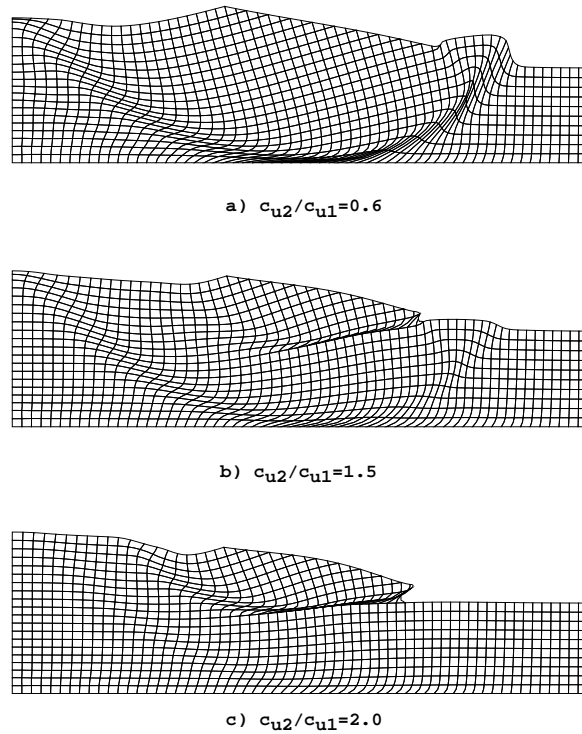
Figure 11. Example 4: Deformed meshes at failure corresponding to the unconverged solution for three different values of c_{u2}/c_{u1}

The previous two examples have shown that in even quite simple cases of soil heterogeneity in the form of layering, complex interactions can occur between conflicting mechanisms which are detected by the finite element approach. For more complicated stability problems involving several soil property groups, such as a zoned earth embankment, numerical approaches are arguably the *only* robust way of generating the minimum factor of safety and indicating the location and shape of the critical mechanism.

15

1.5 Influence of Free Surface and Reservoir Loading on Slope Stability

We now consider the influence of a free-surface within an earth slope and reservoir loading on the outside of a slope as shown in Figure 12.
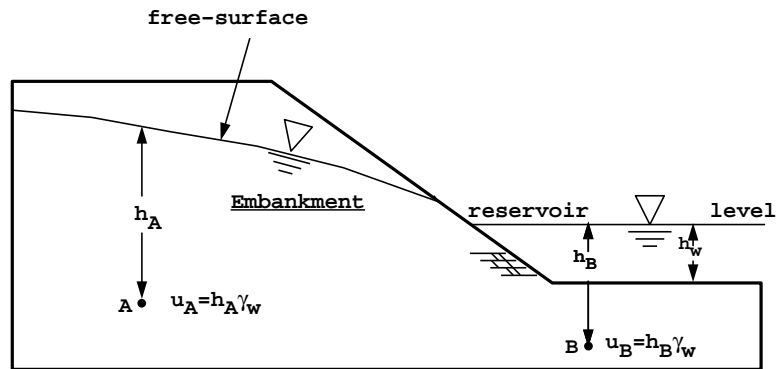

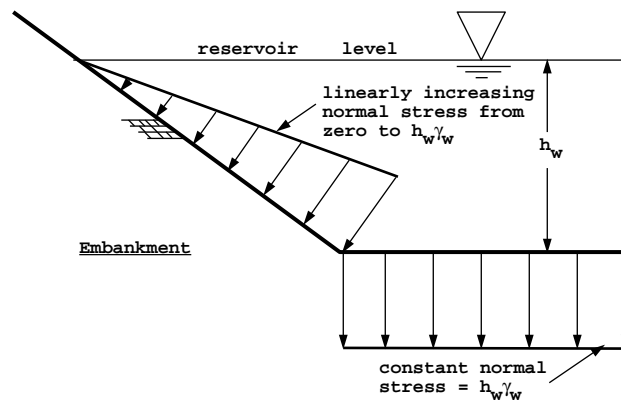**Figure 12.** Slope with free-surface and reservoir loading.

Figure 13. Detail of submerged area of slope beneath free-standing reservoir water showing stresses to be applied to the surface of the mesh as equivalent nodal loads.

Regarding the role of the free-surface, a rigorous approach would firstly involve obtaining a good quality flow net for free-surface flow through the slope, enabling pore pressures to be accurately estimated at any point within the flow region. For the purposes of slope stability analysis however, it is usually considered sufficiently accurate and conservative to estimate pore pressure at a point as the product of the unit weight of water (γ_w) and the *vertical* distance of the point beneath the free-surface. In Figure 12 the pore pressures at two locations, A and B, have been calculated using this assumption.

In the context of finite element analysis, the pore pressures are computed at all submerged (Gauss) points as described above, and subtracted from the *total* normal stresses computed at the same locations following the application of surface and gravity loads. The resulting *effective* stresses are then used in the remaining parts of the algorithm relating to the assessment of Mohr-Coulomb yield and elasto-plastic stress redistribution. Note that the gravity loads are computed using *total* unit weights of the soil.

The external loading due to the reservoir is modelled by applying a normal stress to the face of the slope equal to the water pressure. Thus, as shown in Figure 13, the applied stress increases linearly with water depth and remains constant along the horizontal foundation level. These stresses are converted into equivalent nodal loads on the finite element mesh (see e.g. Appendix I in Smith and Griffiths 1998) and added to the initial gravity loading.

Example 5: Homogeneous slope with horizontal free-surface. Figure 14 shows a similar slope to that analysed in Example 1, but with a horizontal free surface at a depth L below the crest. Using the method described above, the factor of safety of the slope has been computed for several different values of the drawdown ratio (L/H) which has been varied from -0.2 (slope completely submerged with the water level 0.2H above the crest), to 1.0 (water level at the base of the slope). The problem could be interpreted as a "slow" drawdown problem in which a reservoir, initially above the crest of the slope (!), is gradually lowered to the base, with the water level within the slope maintaining the same level. A constant total unit weight of 20kN/m^3 has been assigned to the entire slope, both above and below the water level.
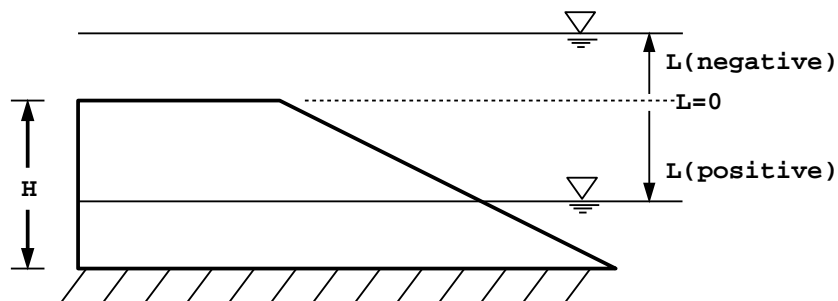
Figure 14. Example 5: "Slow" drawdown problem. Homogeneous slope with a horizontal free surface. Slope angle 26.57^o (2:1), $\phi^{'} = 20^o$, $c^{'}/\gamma H = 0.05$ (above and below free surface).

The interesting result shown in Figure 15 indicates that the factor of safety reaches a *minimum* of $FOS \approx 1.3$ when $L/H \approx 0.7$. A limit equilibrium solution shown on the same figure indicates a similar trend (see e.g. Cousins 1978). The special cases corresponding to $L/H = 0$ and $L/H = 1$ agree well with chart solutions given, respectively, by Morgenstern (1963) (F=1.85), and Bishop and Morgenstern (1960) ($FOS = 1.4$). The fully submerged
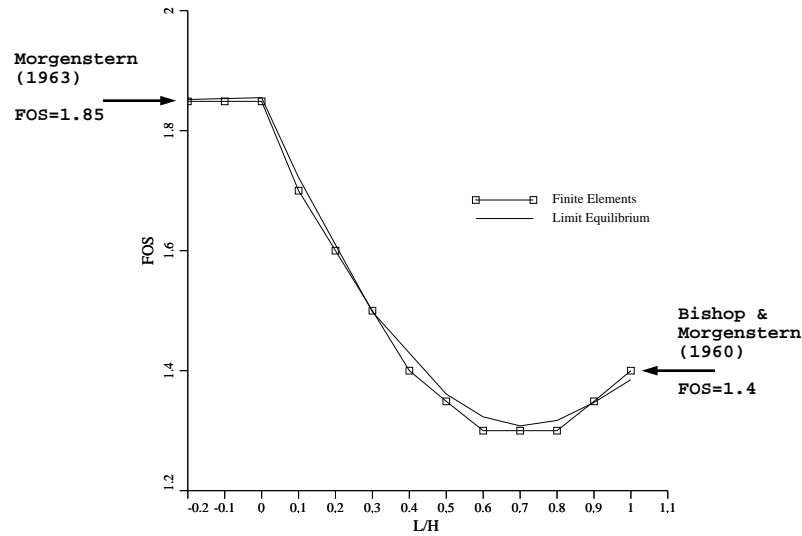
Figure 15. Factor of safety in a "slow" drawdown problem for different values of the drawdown ratio L/H.

slope ($L/H \leq 0$) is more stable than the "dry" slope ($L/H \geq 1$) as indicated by a higher factor of safety.

An explanation of the observed minimum is due to the cohesive strength of the slope (which is unaffected by buoyancy) and the trade-off between soil weight and soil shear strength as the drawdown level is varied. In the initial stages of drawdown ($L/H < 0.7$), the increased weight of the slope has a proportionately greater destabilising effect than the increased frictional strength and the factor of safety falls. At higher drawdown levels ($L/H > 0.7$) however, the increased frictional strength starts to have a greater influence than the increased weight and the factor of safety rises. Other results of this type have been reported by Lane and Griffiths (2000) for a slope which was stable ($FOS > 1$) when "dry" or fully submerged, but became unstable ($FOS < 1$) at a critical value of the drawdown ratio L/H. It should also be pointed out from the horizontal part of the graph in Figure 15, corresponding to $L/H \leq 0$, that the factor of safety for a fully submerged slope is unaffected by the depth of water above the crest.

Excellent agreement with Morgernstern (1963) for "rapid drawdown" problems has also been demonstrated for a range of slopes using this approach by Lane and Griffiths 2000.

Example 6: Two-sided earth embankment. The example given in Figure 16 is of an actual earth dam cross section including a free surface which slopes from the reservoir level to foundation level on the downstream side (Torres and Coffman 1997). For the purposes of this example, the material properties have been made homogeneous. Figure 17 shows the finite element model used for the slope stability analysis (Paice 1997). The boundary conditions consist of vertical rollers on the faces at the left and right ends of the foundation layer with full fixity at the base. It should be noted that the downstream slope of the embankment is slightly steeper than the upstream slope.

18

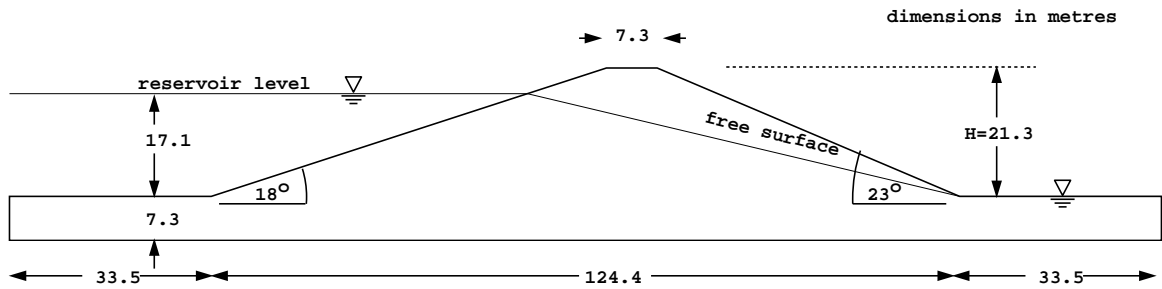**Figure 16.** Example 6: Two-sided earth embankment with a sloping free surface. $\phi' = 37^o$, $c' = 13.8$ kN/m^2, $\gamma = 18.2$ kN/m^3 (above and below WT).
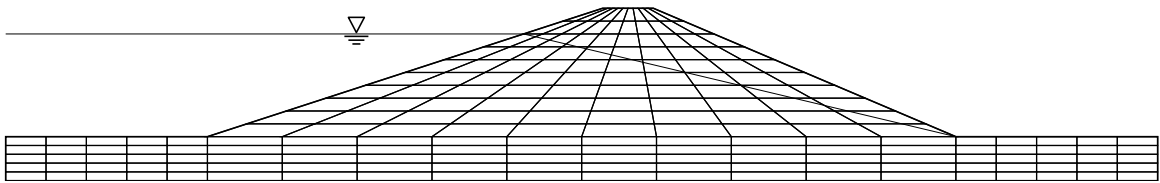

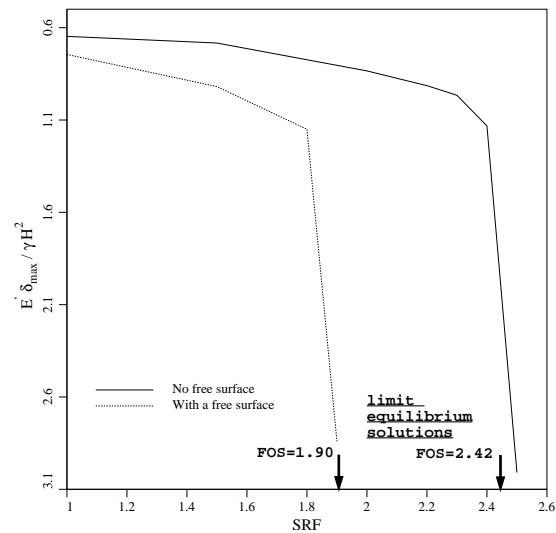**Figure 17.** Example 6: Finite element mesh.

Figure 18. Example 6: SRF vs. Dimensionless displacement.

A second analysis was also performed with no free-surface corresponding to the embankment before the reservoir was filled. Finite element slope stability analysis led to the results shown in Figure 18. Both cases were also solved using a conventional limit equilibrium approach which gave $FOS = 1.90$ with a free surface and $FOS = 2.42$ without a free surface. The limit equilibrium and finite element factors of safety values were in close agreement in both cases.
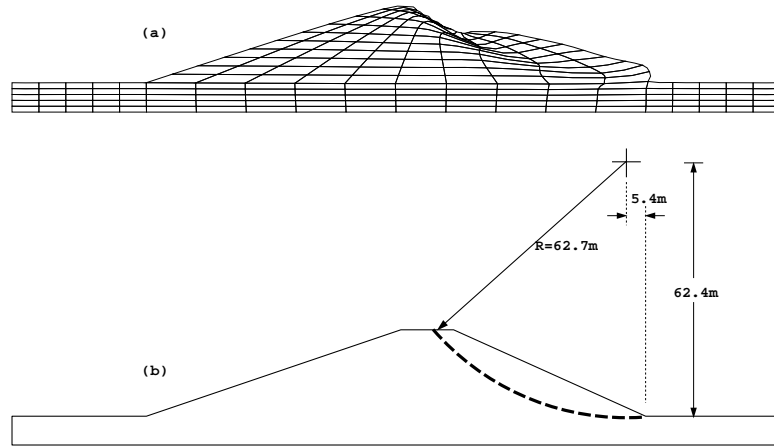
Figure 19. Example 6 with no free surface: (a) Deformed mesh corresponding to the unconverged solution by finite elements, (b) the critical slip circle by limit equilibrium. Both methods give FOS=2.4.
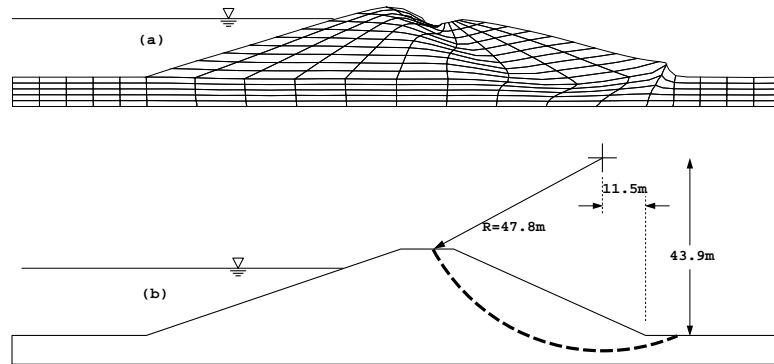
Figure 20. Example 6 with a free surface: (a) Deformed mesh corresponding to the unconverged solution by finite elements, (b) the critical slip circle by limit equilibrium. Both methods give FOS=1.9.

Regarding the critical mechanisms of failure, Figures 19 and 20 show the deformed mesh corresponding to the unconverged finite element solution as compared with the slip circle that gave the lowest factors of safety from the limit equilibrium approach. As expected, the lowest factor of safety occurs on the steeper, downstream side of the embankment in both cases. It should also be noted that both the finite element and limit equilibrium results indicate a toe failure for the case with no free-surface (Figure 19), and a deeper mechanism extending into the foundation layer for the case with a free surface (Figure 20). Figure 21 shows the corresponding displacement vectors from the finite element solutions. Reasonably good agreement between the locations of the failure mechanisms indicated by both types of analysis is indicated.
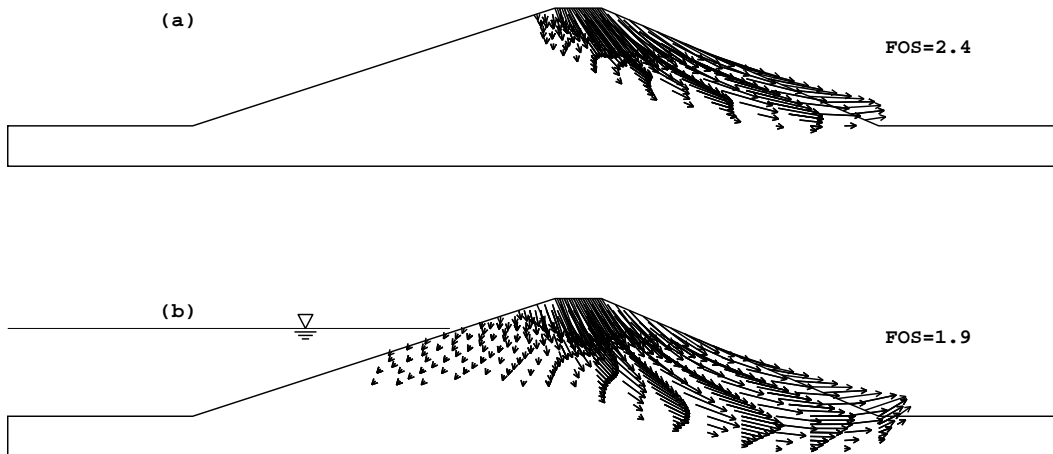
Figure 21. Example 6: Displacement vectors corresponding to the unconverged solution by finite elements, (a) no free surface, (b) with a free surface.

1.6   The Criteria for Computer Aided Analysis

In their 1967 paper Whitman and Bailey looked forward to the future of computer aided analysis for engineers and set criteria by which it could be judged. Their comments were originally addressed to the automation of limit equlibrium methods but they also commented on the then emerging numerical analysis techniques.

They judged that the system must be sufficiently accurate for confidence in its use and appropriate for the parameters being input. Finite element analysis meets these criteria with a degree of accuracy decided by the engineer in designing the model.

It should be possible, in a realistic timescale, to do sufficient trials to examine all the key modes of behaviour; to consider different times in the life of the structure and to vary

parameters during design to test options for cost and efficiency. All this is now possible with FE methods.

Finally the method of human-machine communication must be be user-friendly and readily accessible. This is partly a matter of program design but easily achieved. Graphical output greatly enhances the process of design and analysis over and above that from the numerical results.

Similarly, Chowdhury (1981) in his discussion of Sarma (1979) commented on the perceived reluctance to develop alternatives to limit equilibrium methods for practice when the tools to do so were already available. Since then numerous applications and experience have verified the possibilities offered by finite elements.

The key issues of cost and turnaround time have been overtaken by the falling cost of powerful hardware and processor speeds which now make the FE method available to engineers at less than the cost of their CAD systems. What remains is the concern of powerful tools used wrongly. That is no more true of finite elements after years of application than of limit equilibrium methods which can themselves produce seriously misleading results. Engineering judgement is still essential whichever method is being used.

1.7 Concluding Remarks

The finite element method in conjunction with an elastic-perfectly plastic (Mohr-Coulomb) stress strain model has been shown to be a reliable and robust method for assessing the factor of safety of slopes. One of the main advantages of the finite element approach, is that the factor of safety emerges naturally from the analysis without the user having to comit to any particular form of the mechanism a *priori*.

The finite element approach for determining the factor of safety of slopes has satisfied the criteria for effective computer aided analysis. The widespread use of this method should now be seriously considered by geotechnical practitioners as a more powerful alternative to traditional limit equilibrium methods.

2 A Probabilistic Approach to Slope Stability using Finite Elements

An investigation has been performed into the stability of an undrained clay slope having spatially randomly varying shear strength. The results of the study lead to a direct comparison between the probability of slope failure and the traditional Factor of Safety for a range of statistically defined input shear strength properties. The results highlight the influence of the spatial correlation length, a variable which is routinely omitted from conventional probabilistic studies in geotechnics.

2.1 Introduction

The section presents results obtained using a program developed by Gordon Fenton of Dalhousie University and the author (Griffiths and Fenton 2000), which merges non-linear elasto-plastic finite element analysis with random field theory (e.g. Fenton 1990,

Vanmarcke 1984). Some initial work using this approach has been reported by Paice and Griffiths (1997), however the problem to be considered in this paper is an undrained clay slope ($\phi_u = 0$) of height H with a gradient of 2:1 resting on a foundation layer, also of depth H. A typical finite element mesh is shown in Figure 22.
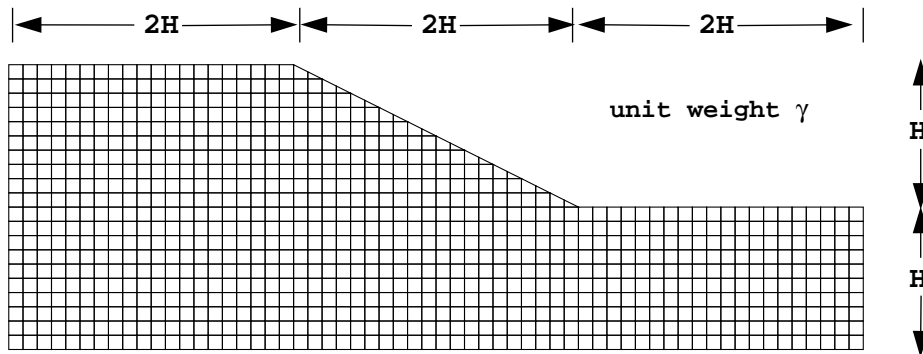
Figure 22. Mesh used for slope stability analyses.

In this study, the variability of the undrained shear strength (c_u) is assumed to be characterized by a lognormal distribution [2] with the parameters shown in Table 2.1.

Table 2.1. Statistical Parameters

		Units
Mean	μ_{c_u}	Stress
Standard Deviation	σ_{c_u}	Stress
Spatial Correlation Length	$\theta_{\ln c_u}$	Length

The mean and standard deviation can conveniently be expressed in terms of the dimensionless coefficient of variation defined as

$$C.O.V._{c_u} = \frac{\sigma_{c_u}}{\mu_{c_u}} \tag{6}$$

Rearranged the following par the actual undrained shear field is assumed lognormally distributed, taking its logarithm yields an "underlying" normally distributed (or Gaussian) field. The spatial correlation length is measured with respect to this underlying field, that is, with respect to $\ln c_u$. In particular, the spatial correlation length ($\theta_{\ln c_u}$) describes the distance over which the spatially random values will tend to be significantly correlated in the underlying Gaussian field. Thus, a large value of $\theta_{\ln c_u}$ will imply a smoothly varying field, while a small value will imply a ragged field. The spatial correlation length can be estimated from a set of shear strength data taken over some spatial

[2] A more detailed discussion of the lognormal distribution is given in Section 5.2 of this report.

region simply by performing the statistical analyses on the log-data. In practice, however, $\theta_{\ln c_u}$ is not much different in magnitude from the correlation length in real space and, for most purposes, θ_{c_u} and $\theta_{\ln c_u}$ are interchangeable given their inherent uncertainty in the first place. In the current study, the spatial correlation length has been non-dimensionalized by dividing it by the height of the embankment H, introducing to the variable $\Theta_{c_u} = \theta_{\ln c_u}/H$.

It should be emphasised that the spatial correlation length is rarely taken into account in routine probabilistic studies relating to geotechnical engineering. In the majority of these cases, a Single Random Variable approach (e.g. Harr 1987, Duncan 2000) is used, which is equivalent to setting $\Theta_{c_u} = \infty$.

It has been suggested (see e.g. Lee *et al* 1983, Kulhawy *et al* 1991 and Duncan 2000) that typical $C.O.V._{c_u}$ values for the undrained shear strength lie in the range 0.1-0.5, however the spatial correlation length is less well documented, especially in the horizontal direction, and may well exhibit anisotropy. While the analysis tools used in this study have the capability of modeling an anisotropic spatial correlation field, all the results presented in this report assume that Θ_{c_u} is isotropic. This is not a severe restriction, since the geometry can often be scaled to achieve the desired spatial correlation structure

2.2 Brief description of the finite element method used

The slope stability analyses use an elastic-perfectly plastic stress-strain law with a Tresca failure criterion similar to that described in the first section of this report. Plastic stress redistribution is accomplished using a viscoplastic algorithm which uses 8-node quadrilateral elements and reduced integration in both the stiffness and stress redistribution parts of the algorithm.

In brief, the analyses involve the application of gravity loading, and the monitoring of stresses at all the Gauss points. If the Tresca criterion is violated, the program attempts to redistribute those stresses to neighboring elements that still have reserves of strength. This is an iterative process which continues until the Tresca criterion and global equilibrium are satisfied at all points within the mesh under quite strict tolerances.

In this study, "failure" is said to have occurred if, for any given realization, the algorithm is unable to converge within 500 iterations. Following a set of 1000 realizations of the Monte-Carlo process the probability of failure is simply defined as the proportion of these realizations that required 500 or more iterations to converge.

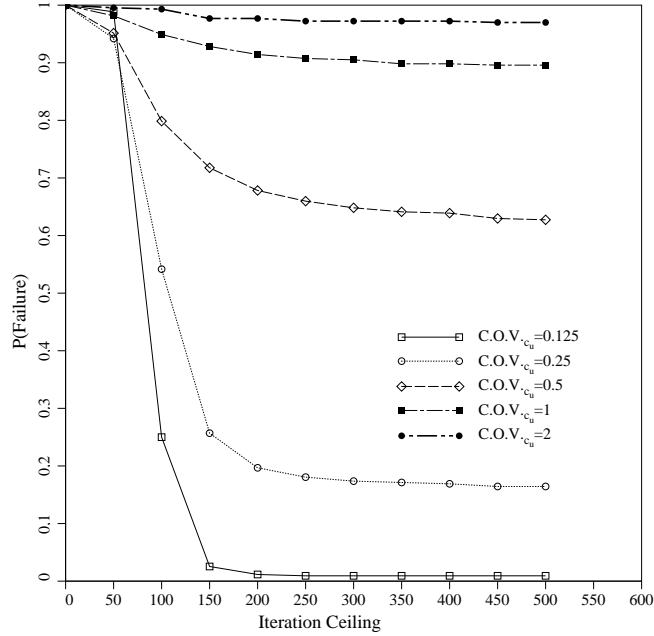While the choice of 500 as the iteration ceiling is subjective, Figure 23 confirms, for the case of $\Theta_{c_u} = 1$, that the probability of failure computed using this criterion is quite stable after about 200 iterations.

2.3 Parametric studies

In the parametric studies described in this section, the mean strength expressed in the form of a Stability Number

$$N_s = \mu_{c_u}/\gamma H \tag{7}$$

24

Figure 23. Probability of failure vs. Iteration Ceiling.

where γ is the unit weight, was given the values 0.15, 0.20, 0.25 and 0.30, and in each case, a range of $C.O.V._{c_u}$ and Θ_{c_u} values were investigated as follows:

$$\Theta_{c_u} = 0.5,\ 1,\ 2,\ 4,\ 8,\ \infty \tag{8}$$
$$C.O.V._{c_u} = 0.125,\ 0.25,\ 0.5,\ 1,\ 2,\ 4$$

To put the probabilistic results in context, Table 2.2 shows the Factor of Safety F from conventional limit equilibrium analysis, for the slope in Figure 22 assuming a homogeneous shear strength defined by the Stability Number N_s.

Table 2.2. Factors of Safety Assuming Homogeneous Soil

N_s	F
0.15	0.88
0.17	1.00
0.20	1.18
0.25	1.47
0.30	1.77

For each set of assumed statistical properties given by $C.O.V._{c_u}$ and Θ_{c_u}, Monte-Carlo simulations were performed, typically involving 1000 repetitions or "realizations" of the shear strength random field and the subsequent finite element analysis. Each realization
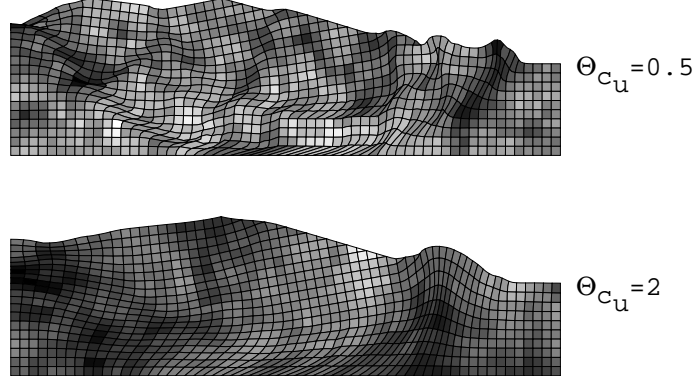
Figure 24. Typical random field realizations. Darker zones indicate weaker soil.

of the random field, while having the same underlying statistics, led to a quite different spatial pattern of shear strength values within the slope.

Figure 24 shows two typical random field realizations and associated failure mechanisms for slopes with $\Theta_{c_u} = 0.5$ and $\Theta_{c_u} = 2$. Notice how the higher Θ_{c_u} gives a more gradually varying shear strength over space and a smoother failure surface.

2.4 Single random variable approach

It is instructive to consider the special case of $\Theta_{c_u} = \infty$, which implies that each realization of the Monte-Carlo process gives a uniform strength, the same everywhere, but with the strength varying from one realization to the next according to the governing lognormal distribution. The probability of failure in such a case is simply equal to the probability that the Stability Number N_s will be below 0.17, the value that would give a Factor of Safety of unity.

For example, if $\mu_{c_u} = 0.25\gamma H$ and $\sigma_{c_u} = 0.125\gamma H$, corresponding to $C.O.V._{c_u} = 0.5$, the statistics of the Stability Number are therefore given by $\mu_{N_s} = 0.25$, $\sigma_{N_s} = 0.125$ and $C.O.V._{N_s} = 0.5$.

From standard relationships, the mean and standard deviation of the underlying *normal* distribution of the Stability Number are given by:

$$\sigma_{\ln N_s} = \sqrt{\ln\left\{1 + \left(\frac{\sigma_{N_s}}{\mu_{N_s}}\right)^2\right\}} \tag{9}$$

$$\mu_{\ln N_s} = \ln\mu_{N_s} - \frac{1}{2}\sigma_{\ln N_s}^2 \tag{10}$$

hence $\mu_{\ln N_s} = -1.498$ and $\sigma_{\ln N_s} = 0.472$.

The probability of failure is therefore given by:

$$p(N_s < 0.17) = \Phi\left(\frac{\ln 0.17 - \mu_{\ln N_s}}{\sigma_{\ln N_s}}\right) \tag{11}$$

$$= 0.281 \tag{12}$$

where Φ is the cumulative normal distribution function. The relationship between the Factor of Safety (assuming a constant shear strength equal to μ_{c_u}) and the probability of failure assuming a Single Random Variable ($\Theta_{c_u} = \infty$) is summarized in Figure 25 for a range of $C.O.V._{c_u}$ values.
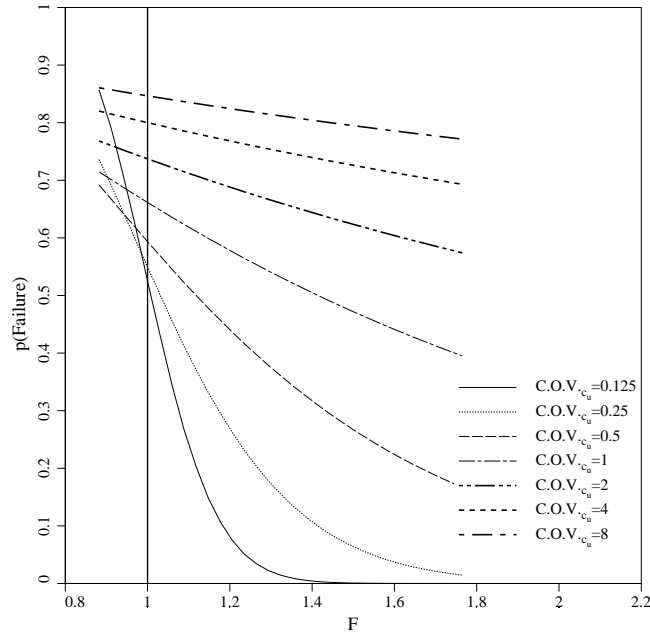
Figure 25. Factor of Safety vs. Probability of Failure. Single random variable approach, $\Theta_{c_u} = \infty$

Apart from the rather obvious conclusion that the probability of failure goes up as the Factor of Safety goes down, it is also clear that for the majority of cases, the probability of failure also goes up as the $C.O.V._{c_u}$ of the shear strength increases. This result is not necessarily intuitive, since soil with a higher $C.O.V._{c_u}$ contains elements that are much weaker *and* much stronger than the mean. The result indicates however, that the weaker elements dominate the stability calculation.

The only exception to this trend occurs when the mean strength indicates a Factor of Safety of *less* than unity. As shown in Figure 25, the probability of failure in such cases is understandably high, however the role of $C.O.V._{c_u}$ has the opposite effect to that described above, with lowest values of $C.O.V._{c_u}$ tending to give the highest values of the probability of failure.

27

It is interesting to note that using this approach, a slope with a Factor of Safety of 1.50, based on the mean strength, would have a probability of failure as high as 27% if $C.O.V._{c_u} = 0.5$, the upper limit of the recommended range of Lee et al (1983) and others.

2.5   Random field approach.

The code developed by the authors enables a random field of shear strength values to be generated and subsequently mapped onto the finite element mesh. In a random field, the value assigned to each cell (or finite element in this case) is itself a random variable, thus the mesh of Figure 22 which has 910 finite elements consists of 910 random variables. The random variables can be correlated to one another by controlling the spatial correlation length Θ_{c_u} as described previously, hence the single random variable approach discussed in the previous section can now be viewed as just a special case of a much more powerful analytical tool.

Figures 26 and 27 show the effect of the spatial correlation length Θ_{c_u} on a soil with a Factor of Safety of 1.47 (based on the mean strength) for a range of $C.O.V._{c_u}$ values. Figure 26 clearly indicates two branches relating to the value of $C.O.V._{c_u}$. For low values of $0 < C.O.V._{c_u} \leq 0.5$, the probability of failure increases as Θ_{c_u} increases, indicating that the Single Random Variable approach in which $\Theta_{c_u} = \infty$ is conservative. For high values of $1 \leq C.O.V._{c_u}$ quite the reverse trend is apparent, with the higher values of Θ_{c_u} tending to $underestimate$ the probability of failure.
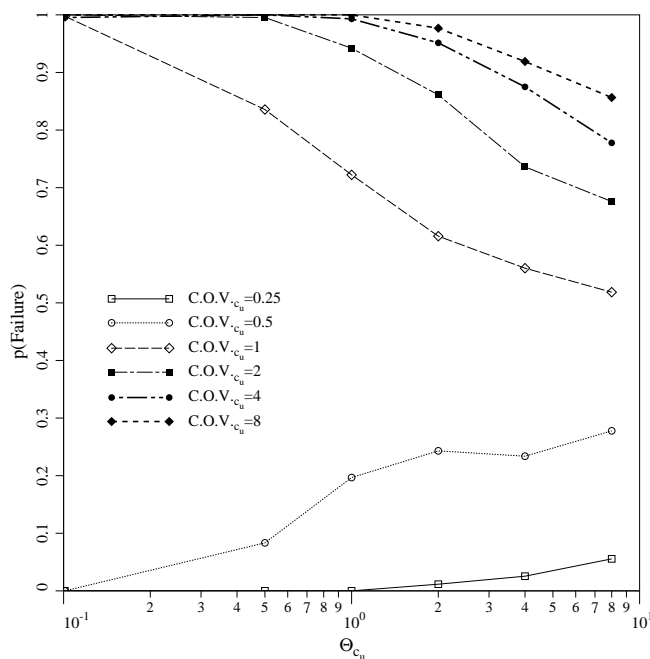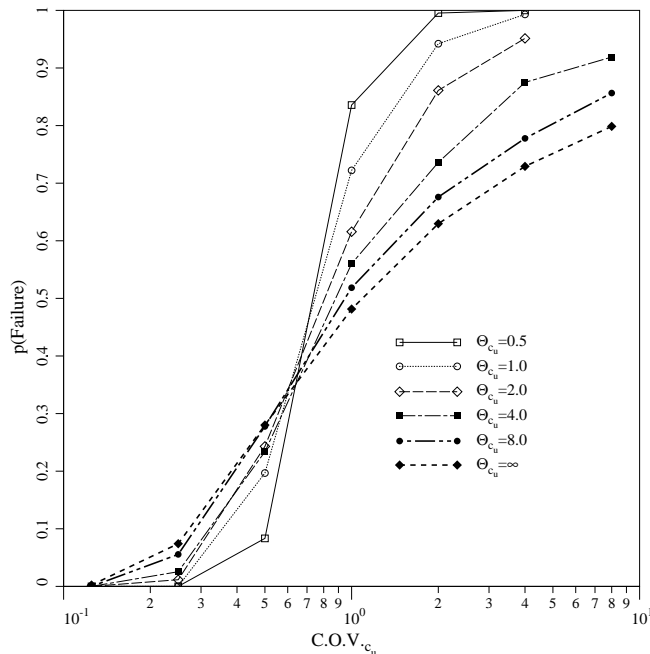

**Figure 26.** Influence of Θ_{c_u} on a slope with F=1.47.

28

Figure 27. Influence of $C.O.V._{c_u}$ on a slope with F=1.47.

Figure 27 shows an alternative representation of the same data with $C.O.V._{c_u}$ plotted along the abscissa. This figure shows more clearly how $\Theta_{c_u} = \infty$ will tend to overestimate the probability of failure for low $C.O.V._{c_u}$ values and underestimate it for high values. It is also of interest to note the sensitivity of the probability of failure to the value of $C.O.V._{c_u}$ for low levels of correlation. For example, the line corresponding to $\Theta_{c_u} = 0.5$ rises steeply from zero to 100% probability of failure within the relatively narrow band of $0.25 < C.O.V._{c_u} < 2$. For even smaller values of Θ_{c_u} the rise was observed to be even more dramatic, although these results are not presented here. A further point of interest from Figure 27 is that all the lines appear to coincide at approximately the same value of $C.O.V._{c_u} \approx 0.65$, implying that at this level of shear strength variance, the probability of failure is independent of Θ_{c_u}.

The observations made with respect to Figures 26 and 27 were for the particular case of a mean shear strength that would have given a Factor of Safety of 1.47. The results from further analyses of a range of mean shear strength values corresponding to the Stability Numbers in Table 2.2 are shown in Figure 28. In order to reduce the number of variables, only the results assuming $C.O.V._{c_u} = 0.5$ are shown.

Figure 28 indicates another type of "cross over" with respect to the Factor of Safety. For the given value of $C.O.V._{c_u} = 0.5$, the Single Random Variable approach corresponding to $\Theta_{c_u} = \infty$ appears to overestimate the probability of failure for slopes with relatively high deterministic Factors of Safety ($F > 1.4$) and underestimate it for lower Factors of Safety ($F < 1.4$).

29
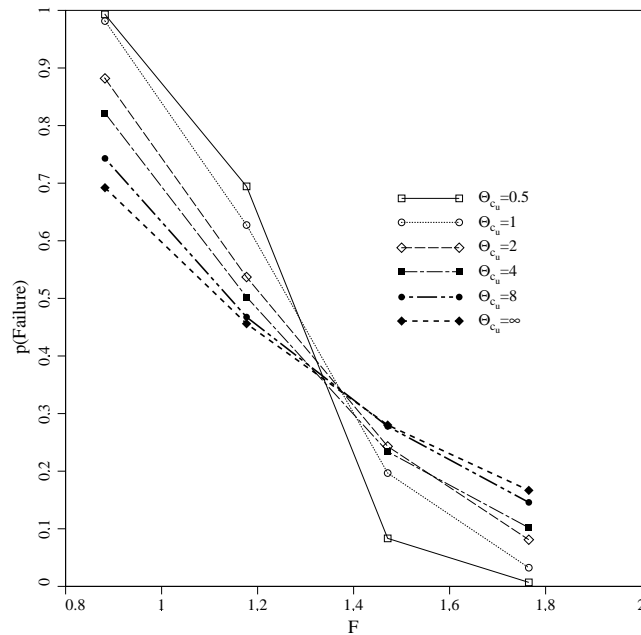
Figure 28. Influence of Θ_{c_u} on the Probability of Failure for a range of deterministic Factors of Safety ($C.O.V._{c_u} = 0.5$)

.

2.6 Concluding remarks

The section has shown that soil strength heterogeneity in the form of a spatially varying lognormal distribution can significantly affect the stability of a slope of undrained clay when viewed in a probabilistic context. In this paper, particular attention was paid to the validity of treating the heterogeneity as a Single Random Variable which was shown to be a special case of the authors' formulation corresponding to an infinite correlation length of $\Theta_{c_u} = \infty$.

The following more specific observations can be made from the results presented in this paper:

1. For the slope considered in this study with a Factor of Safety of 1.47 based on the mean strength, the Single Random Variable approach gave conservative estimates of the probability of failure for Coefficient of Variation values in the "typical" range of $0 < C.O.V._{c_u} < 0.5$. For higher values of $C.O.V._{c_u}$ however, the Single Random Variable approach gave unconservative estimates.
2. For the slope considered in this study with $C.O.V._{c_u} = 0.5$, the Single Random Variable approach gave conservative estimates of the probability of failure for higher Factors of Safety in the approximate range $F > 1.4$ and unconservative estimates for lower Factors of Safety when $F < 1.4$.

More work remains to be done in this area, but the implications of this study are that the Single Random Variable approach is an acceptable guide to probabilistic slope

30

stability providing the mean strength indicates a relatively high Factor of Safety. For more critical cases, in which the mean strength indicates a Factor of Safety closer to unity, the Single Random Variable approach can give an unconservative estimate of the probability of failure, i.e. *lower* than the "true" value.

A final comment relates to the influence of the Coefficient of Variation of the soil shear strength. While increasing the value of $C.O.V._{c_u}$ introduces both stronger and weaker zones of soil into the slope, the weaker soil always dominates the overall performance leading to a *less* stable slope.

3 Excavation Software

Heterogeneity in geotechnical problems can also occur in the form of voids caused by tunneling and excavation.

All the slope stability analyses described in the first two sections of this report assumed the slope was initially weightless and then suddenly subjected to gravity loading in a single increment. While this is unrealistic, evidence was produced in Figure 3 showing that the factor of safety is insensitive to the rate of gravity loading (e.g. Lechman 2000).

The basic slope stability approach however takes no account of construction sequence in the form of "building up" or "excavating down". The text by Smith and Griffiths (1998) contains Program 6.9 (construction of an embankment) and Program 6.10 (excavation of an embankment). In this section, the excacation program 6.10 is briefly revisited, and a slightly modified version of the code is included. Some examples of tunneling type excavation are then presented. The interested reader is referred to Brown and Booker (1985) and Smith and Ho (1992) for more background on the excavation algorithm.

3.1 Excavation loads
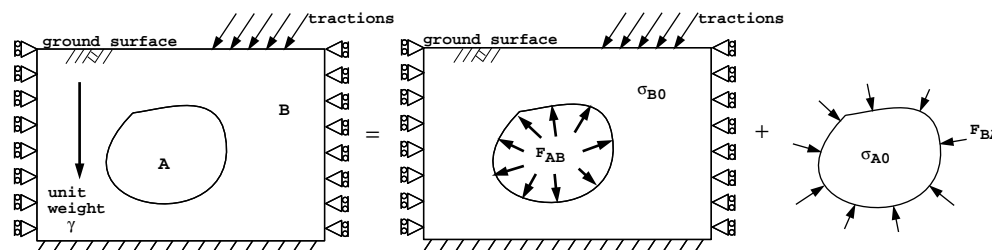

Figure 29. Excavation forces

.

The aim of an analysis is that when a portion of material is excavated, either in open excavations or an enclosed tunnel, forces must be applied along the excavated surface such that:

– The remaining material experiences the correct unloading effect.

– The new "free surface" is stress free.

Figure 29 shows a 2-d block of soil from which a zone of material is to be excavated. The soil to be removed is zone A and the surrounding soil that will remain after excavation is zone B. The initial stresses in the zone to be removed and the surrounding soil are labelled σ_{A0} and σ_{B0} respectively. Any self-weight and external loads are taken into account in forming these stresses prior to the removal of A. Since both bodies are in equilibrium, forces F_{AB} must be applied to body B by body A to maintin σ_{B0} and, similarly, F_{BA} must act on body A as shown in Figure 29. Forces F_{AB} and F_{BA} are equal and opposite. In general therefore, the forces to be applied to the excavated boundaries depend on the initial stress state in the excavated material and its self-weight. It can be shown that (e.g. Brown and Booker 1985):

$$F_{AB} = \int_{V_A} \mathbf{B}^T \sigma_{A0} dV_A + \gamma \int_{V_A} \mathbf{N}^T dV_A \tag{13}$$

where $\mathbf{B}$ is the strain-displacement matrix, $\mathbf{N}$ the element shape functions, and V_A and γ are respectively the volume and unit weight of the excavated material.

3.2 Listing and sample data for excavation program

The following listing represents a modified version of Program 6.10 from the text by Smith and Griffiths (1998). The modified program is called `p610_1.f90` and this, together with all other programs, libraries and data from the text, can be obtained from the author's web site at:

<center>http://www.mines.edu/fs_home/vgriffit/</center>

then under the heading "SOFTWARE FROM TEXTBOOKS", click on "Programming the finite element method" and click on "chap6".

The general approach for each excavation step is to compute the loads to be applied to the excavation boundary using equation (13). The properties of the elements in the mesh are then modified by setting Young's Modulus of excavated elements to zero. Although the total number of nodes in the mesh remains constant throughout, the introduction of "air" elements involves a re-numbering of the active freedoms within the mesh, and hence a full re-assembly of the global stiffness matrix at each excavation step. It should also be noted that to avoid zeros on the diagonal of the modified global stiffness matrix, any freedoms attached to nodes that become completely surrounded by "air", must be removed from the analysis and not assembled into the global stiffness matrix.

The reader is referred to the original program 6.10 for the meaning of most variable names, however the main changes in the current version may be summarised as follows:

– Only the excavated element numbers need to be given as data. The nodes affected by the excavation are computed automatically. New variables include:
  noexe–the number of elements to be removed at each excavation step,

`ntote`–a running total of the total number of elements excavated,
`exele(noexe)`–the element numbers to be removed at each excavation step,
`totex(ntote)`–all the element numbers removed.

- Subroutines `mesh_exc.f90`, `dis_exc.f90`, `vec_exc.f90` have been developed to generate PostScript output files corresponding to, repectively, the undeformed mesh, the deformed mesh and the nodal displacment vectors. All figures correspond to the situation following the final excavation step, whether converged or not. These subroutines have not been included in the listing that follows, but are appended to the end of the program available on the web as described above.
- The program is quite general, and reads the coordinates and connectivity of the initial mesh via data. The program also permits different material property groups in the style of Program 6.8.
- Some minor cosmetic changes have been made to allow data control of which specific nodal displacements are to be printed following each excavation step.

The data file that follows represents the same analysis presented in the text with Program 6.10, in which a vertical cut in undrained clay is excavated in two stages as shown in Figure 30. The rather crude mesh is used for demonstration purposes only. The nodes are indicated by numbers with circles around them and element numbers are indicated in the middle of each element. The side boundary conditions are rollers (vertical movement only) and the base is fixed. The meanings of the input variable names are defined in Table 3.1.

Table 3.1. Input variable names

nels	number of elements
nn	number of nodes
limit	iteration ceiling
tol	iteration tolerance
epk0	"at rest" earth pressure coefficient
nprops	number of properties (6)
np_types	number of property groups
prop(nprop,np_types)	properties (ϕ, c, ψ, γ, E, ν)
nouts	number of output nodes
no(nouts)	output node numbers
g_coord(2,nn)	nodal coordinates (x, y)
g_num(8,nels)	element node numbers
nr	number of restrained nodes
k,nf(:,k)	node number and fixity (0 or 1), (nr-times)
layers	number of excavations
incs	increments per excavation
noexe	number of elements to be removed
exele(noexe)	element numbers to be removed
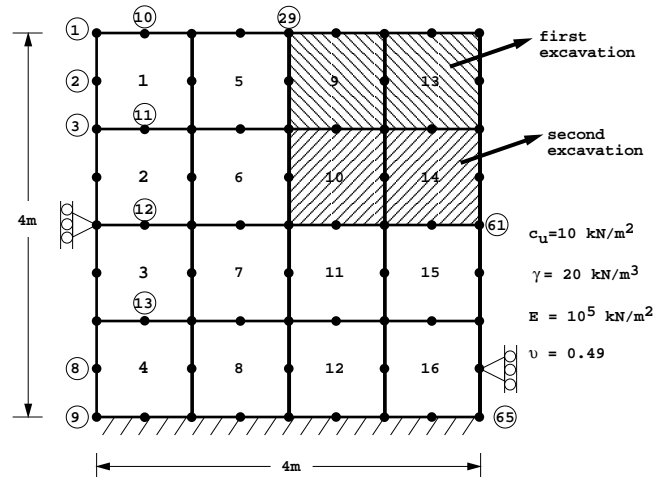
Figure 30. Test excavation problem

.

<u>**Data File** `p610_1.dat`</u>

```
nels   nn   limit   tol    epk0
 16    65    250    .0001   1.


nprops   np_types
  6         1


prop
0.0   10.0   0.0   20.0  1.e5  0.49


nouts
2


no
29 61


g_coord
0.0000E+00   0.0000E+00
0.0000E+00  -0.5000E+00
0.0000E+00  -0.1000E+01
0.0000E+00  -0.1500E+01
0.0000E+00  -0.2000E+01
0.0000E+00  -0.2500E+01
0.0000E+00  -0.3000E+01
0.0000E+00  -0.3500E+01
0.0000E+00  -0.4000E+01
0.5000E+00   0.0000E+00
0.5000E+00  -0.1000E+01
```

34

```
0.5000E+00 -0.2000E+01
0.5000E+00 -0.3000E+01
0.5000E+00 -0.4000E+01
0.1000E+01  0.0000E+00
0.1000E+01 -0.5000E+00
0.1000E+01 -0.1000E+01
0.1000E+01 -0.1500E+01
0.1000E+01 -0.2000E+01
0.1000E+01 -0.2500E+01
0.1000E+01 -0.3000E+01
0.1000E+01 -0.3500E+01
0.1000E+01 -0.4000E+01
0.1500E+01  0.0000E+00
0.1500E+01 -0.1000E+01
0.1500E+01 -0.2000E+01
0.1500E+01 -0.3000E+01
0.1500E+01 -0.4000E+01
0.2000E+01  0.0000E+00
0.2000E+01 -0.5000E+00
0.2000E+01 -0.1000E+01
0.2000E+01 -0.1500E+01
0.2000E+01 -0.2000E+01
0.2000E+01 -0.2500E+01
0.2000E+01 -0.3000E+01
0.2000E+01 -0.3500E+01
0.2000E+01 -0.4000E+01
0.2500E+01  0.0000E+00
0.2500E+01 -0.1000E+01
0.2500E+01 -0.2000E+01
0.2500E+01 -0.3000E+01
0.2500E+01 -0.4000E+01
0.3000E+01  0.0000E+00
0.3000E+01 -0.5000E+00
0.3000E+01 -0.1000E+01
0.3000E+01 -0.1500E+01
0.3000E+01 -0.2000E+01
0.3000E+01 -0.2500E+01
0.3000E+01 -0.3000E+01
0.3000E+01 -0.3500E+01
0.3000E+01 -0.4000E+01
0.3500E+01  0.0000E+00
0.3500E+01 -0.1000E+01
0.3500E+01 -0.2000E+01
0.3500E+01 -0.3000E+01
0.3500E+01 -0.4000E+01
0.4000E+01  0.0000E+00
0.4000E+01 -0.5000E+00
0.4000E+01 -0.1000E+01
0.4000E+01 -0.1500E+01
```

```
0.4000E+01 -0.2000E+01
0.4000E+01 -0.2500E+01
0.4000E+01 -0.3000E+01
0.4000E+01 -0.3500E+01
0.4000E+01 -0.4000E+01

g_num
  3    2    1   10   15   16   17   11
  5    4    3   11   17   18   19   12
  7    6    5   12   19   20   21   13
  9    8    7   13   21   22   23   14
 17   16   15   24   29   30   31   25
 19   18   17   25   31   32   33   26
 21   20   19   26   33   34   35   27
 23   22   21   27   35   36   37   28
 31   30   29   38   43   44   45   39
 33   32   31   39   45   46   47   40
 35   34   33   40   47   48   49   41
 37   36   35   41   49   50   51   42
 45   44   43   52   57   58   59   53
 47   46   45   53   59   60   61   54
 49   48   47   54   61   62   63   55
 51   50   49   55   63   64   65   56

nr
25

k,nf(:,k),i=1,nr
 1 0 1  2 0 1  3 0 1  4 0 1  5 0 1  6 0 1  7 0 1  8 0 1  9 0 0
14 0 0 23 0 0 28 0 0 37 0 0 42 0 0 51 0 0 56 0 0
57 0 1 58 0 1 59 0 1 60 0 1 61 0 1 62 0 1 63 0 1 64 0 1 65 0 0

layers incs
2        5

noexe
2
exele
9  13

noexe
2
exele
10  14
```

Program p610_1.f90

```fortran
program p610_1
!-------------------------------------------------------------------------
!      A more general version of Program 6.10.
!      Plane strain of an elastic-plastic (Mohr-Coulomb) solid
!      using 8-node quadrilateral elements, viscoplastic strain method.
!      Construction of an excavation in stages introducing ''air'' elements
!
!      General program permitting any shape of initial mesh with
!      multiple property groups if required.
!-------------------------------------------------------------------------
 use main
 use geom
 implicit none
 integer::nels,neq,nband,nn,nr,nip=4,nodof=2,nod=8,nst=4,ndof,            &
          i,k,iel,iters,limit,incs,iy,ndim=2,layers,ii,iq,noexe,nprops,   &
          np_types,jj,nodex,modex,ncheck,ntote,nouts
 logical::converged
 character(len=15)::element='quadrilateral'
 real::det,phi,psi,c,gama,dt,ddt,f,dsbar,dq1,dq2,dq3,lode_theta,sigm,pi,  &
       snph,e,v,epk0,tol
!----------------------------- dynamic arrays----------------------------------
 real,allocatable::kb(:,:),exc_loads(:),points(:,:),bdylds(:),tot_d(:,:),  &
                   evpt(:,:,:),oldis(:),loads(:),dee(:,:),coord(:,:),        &
                   fun(:),jac(:,:),weights(:),der(:,:),deriv(:,:),bee(:,:),&
                   km(:,:),eld(:),eps(:),bload(:),eload(:),erate(:),        &
                   g_coord(:,:),prop(:,:),evp(:),devp(:),m1(:,:),m2(:,:),   &
                   m3(:,:),flow(:,:),tensor(:,:,:),gc(:),s(:)
 integer,allocatable::nf(:,:),g(:),num(:),g_num(:,:),etype(:),solid(:),     &
                   lnf(:,:),exele(:),totex(:),no(:)
!-----------------------input and initialisation--------------------------
 open(10, file = 'fe90.dat')
 open(11, file = 'fe90.res')
!
 read(10,*)nels,nn,limit,tol,epk0
 read(10,*)nprops,np_types
 allocate(prop(nprops,np_types),etype(nels))
 read(10,*)prop
 etype=1
 if(np_types>1)read(10,*)etype
 read(10,*)nouts
 ndof=nod*nodof
!
 write(11,'(a,i5)')"The total number of elements is ",nels
 allocate(nf(nodof,nn),points(nip,ndim),weights(nip),g_coord(ndim,nn),     &
          num(nod),dee(nst,nst),evpt(nst,nip,nels),coord(nod,ndim),         &
          fun(nod),solid(nels),jac(ndim,ndim),der(ndim,nod),               &
          deriv(ndim,nod),g_num(nod,nels),bee(nst,ndof),km(ndof,ndof),     &
```

```
              eld(ndof),eps(nst),totex(nels),bload(ndof),eload(ndof),          &
              erate(nst),evp(nst),devp(nst),g(ndof),m1(nst,nst),m2(nst,nst),    &
              m3(nst,nst),flow(nst,nst),s(nst),tot_d(nodof,nn),gc(ndim),        &
              tensor(nst,nip,nels),lnf(nodof,nn),no(nouts))
!------ nf is an index array of 1s and 0s : lnf is the local nf  --------------
 read(10,*)no
 solid=1
!-------------------- read geometry and connectivity ----------------------
 read(10,*)g_coord
 read(10,*)g_num
 nf=1
 read(10,*)nr
 if(nr>0)read(10,*)(k,nf(:,k),i=1,nr)
 lnf=nf
 call formnf(lnf)
 neq=maxval(lnf)
 write(11,'(a,i5)')"The total possible number of equations is:",neq
 pi=acos(-1.)
!-------- set up the global node numbers and global nodal coordinates ---------
!--------------- loop the elements to set starting stresses ------------------
 call sample(element,points,weights)
 elements_0: do iel=1,nels
   num=g_num(:,iel)
   coord=transpose(g_coord(:,num))
   gama=prop(4,etype(iel))
   gauss_pts_0: do i=1,nip
     call shape_fun(fun,points,i)
     gc=matmul(fun,coord)
     tensor(2,i,iel)=gc(2)*gama
     tensor(1,i,iel)=epk0*tensor(2,i,iel)
     tensor(4,i,iel)=tensor(1,i,iel)
     tensor(3,i,iel)=0.0
   end do gauss_pts_0
 end do elements_0
 write(11,'(a)')"Global coordinates "
 do k=1,nn
   write(11,'(a,i5,a,2e12.4)')"Node",k,"         ",g_coord(:,k)
 end do
 write(11,'(a)')"Global node numbers "
 do k=1,nels
   write(11,'(a,i5,a,8i5)')"Element ",k,"           ",g_num(:,k)
 end do
 tot_d=0.0
 ntote=0
! ---------------------  excavate a layer ----------------------------------
 read(10,*)layers,incs
 layer_number: do ii=1,layers
   write(*,*)"Excavation number",ii
   write(11,'(//,a,i3)')"Excavation number",ii
```

```
!------------------  read elements to be removed ----------------------------
!----------------- program computes excavated nodes ----------------------
   read(10,*)noexe
   ntote=ntote+noexe
   allocate(exele(noexe))
   read(10,*)exele
   totex(ntote-noexe+1:ntote)=exele
   solid(exele)=0
!
   do i=1,noexe
     do k=1,nod
       nodex=0
       ncheck=g_num(k,exele(i))
       do iel=1,nels
         modex=0
         do jj=1,ntote
           if(iel==totex(jj))then
             modex=1
             exit
           end if
         end do
         if(modex==1)cycle
         do jj=1,nod
           if(ncheck==g_num(jj,iel))then
             nodex=1
             exit
           end if
         end do
         if(nodex==1)exit
       end do
       if(nodex==0)nf(:,ncheck)=0
     end do
   end do
!
   lnf=nf
   call formnf(lnf)
   neq=maxval(lnf)
   nband=0
!--------- recalculate the number of freedoms neq and half-bandwidth nband ----
   elements_1: do iel=1,nels
     num=g_num(:,iel)
     call num_to_g(num,lnf,g)
     if(nband < bandwidth(g))nband=bandwidth(g)
   end do elements_1
   write(11,'(/,3(a,i5))')                                         &
   "There are ",neq, " freedoms and nband is",nband," in step",ii
   allocate(kb(neq,nband+1),exc_loads(0:neq),bdylds(0:neq),oldis(0:neq),   &
           loads(0:neq))
   kb=0.0
```

```
    exc_loads=0.0
!-------------------- calculate excavation load --------------------------
    elements_2: do iel=1,noexe
      iq=exele(iel)
      gama=prop(4,etype(iq))
      bload=0.0
      eld=0.0
      num=g_num(:,iq)
      call num_to_g(num,lnf,g)
      coord=transpose(g_coord(:,num))
      gauss_pts_2: do i=1,nip
        call shape_fun(fun,points,i)
        call shape_der(der,points,i)
        jac=matmul(der,coord)
        det=determinant(jac)
        call invert(jac)
        deriv=matmul(jac,der)
        call beemat(bee,deriv)
        s=tensor(:,i,iq)
        eload=matmul(s,bee)
        bload=bload+eload*det*weights(i)
        eld(2:ndof:2)=eld(2:ndof:2)+fun(:)*det*weights(i)
      end do gauss_pts_2
      exc_loads(g)=exc_loads(g)+eld*gama+bload
    end do elements_2
    exc_loads(0)=0.0
!----------------- element stiffness integration and assembly-----------------
    dt=1.e20
    elements_3: do iel=1,nels
      if(solid(iel)==0)then
        e=0.0
      else
        phi=prop(1,etype(iel))
        e=prop(5,etype(iel))
        v=prop(6,etype(iel))
        snph=sin(phi*pi/180.)
        ddt=(4.*(1.+v)*(1.-2.*v))/(e*(1.-2.*v+snph*snph))
        if(ddt<dt)dt=ddt
      end if
      km=0.0
      eld=0.0
      call deemat(dee,e,v)
      num=g_num(:,iel)
      call num_to_g(num,lnf,g)
      coord=transpose(g_coord(:,num))
      gauss_pts_3: do i=1,nip
        call shape_der(der,points,i)
        jac=matmul(der,coord)
        det=determinant(jac)
```

```
      call invert(jac)
      deriv=matmul(jac,der)
      call beemat(bee,deriv)
      km=km+matmul(matmul(transpose(bee),dee),bee)*det*weights(i)
    end do gauss_pts_3
    call formkb(kb,km,g)
  end do elements_3
!--------------- factorise l.h.s. -------------------------------------------
  call cholin(kb)
!----------------- factor excavation load by incs---------------------------
  exc_loads=exc_loads/incs
!------------ apply excavation loads incrementally -------------------------
  load_incs: do iy=1,incs
    write(*,*)"Increment no",iy
    iters=0
    oldis=0.0
    bdylds=0.0
    evpt=0.0
!------------------------  iteration loop -----------------------------------
    its: do
      iters=iters+1
      write(*,*)"iteration",iters
      loads=exc_loads+bdylds
      call chobac(kb,loads)
!------------------------  check convergence -------------------------------
      call checon(loads,oldis,tol,converged)
      if(iters==1)converged=.false.
      if(converged.or.iters==limit)then
        bdylds=0.0
        do iq=1,nn
        do i=1,nodof
          if(lnf(i,iq)/=0)tot_d(i,iq)=tot_d(i,iq)+loads(lnf(i,iq))
        end do
        end do
      end if
!---------------------- go round the Gauss Points --------------------------
      elements_4: do iel=1,nels
        phi=prop(1,etype(iel))
        c=prop(2,etype(iel))
        psi=prop(3,etype(iel))
        e=prop(5,etype(iel))
        v=prop(6,etype(iel))
        if(solid(iel)==0)e=0.0
        bload=0.0
        call deemat(dee,e,v)
        num=g_num(:,iel)
        call num_to_g(num,lnf,g)
        coord=transpose(g_coord(:,num))
        eld=loads(g)
```

```
          gauss_pts_4: do i=1,nip
            call shape_der(der,points,i)
            jac=matmul(der,coord)
            det=determinant(jac)
            call invert(jac)
            deriv=matmul(jac,der)
            call beemat(bee,deriv)
            eps=matmul(bee,eld)
            eps=eps-evpt(:,i,iel)
            s=tensor(:,i,iel)+matmul(dee,eps)
!---------------------- air element stresses are zero ------------------------
            if(solid(iel)==0)s=0.0
            call invar(s,sigm,dsbar,lode_theta)
!-------------------- check whether yield is violated -----------------------
            call mocouf(phi,c,sigm,dsbar,lode_theta,f)
            if(converged.or.iters==limit)then
              devp=s
            else
              if(f>=0.0)then
                call mocouq(psi,dsbar,lode_theta,dq1,dq2,dq3)
                call formm(s,m1,m2,m3)
                flow=f*(m1*dq1+m2*dq2+m3*dq3)
                erate=matmul(flow,s)
                evp=erate*dt
                evpt(:,i,iel)=evpt(:,i,iel)+evp
                devp=matmul(dee,evp)
              end if
            end if
            if(f>=0.0.or.(converged.or.iters==limit))then
              eload=matmul(devp,bee)
              bload=bload+eload*det*weights(i)
            end if
!--------------- if appropriate update the Gauss point stresses ---------------
            if(converged.or.iters==limit)tensor(:,i,iel)=s
          end do gauss_pts_4
!------------------   compute the total bodyloads vector --------------------
          bdylds(g)=bdylds(g)+bload
          bdylds(0)=0.0
        end do elements_4
        if(converged.or.iters==limit)exit
      end do its
      write(11,'(a,i3,a,i5,a)')"Increment",iy," took",iters," iterations to converge"
      if(iy==incs.or.iters==limit)then
        write(11,'(a)')"The displacements are :"
        do i=1,nouts
          write(11,'(i5,2e12.4)')no(i),tot_d(:,no(i))
        end do
      exit
      end if
```

```
   end do load_incs
   loads(lnf(1,:))=tot_d(1,:)
   loads(lnf(2,:))=tot_d(2,:)
   call mesh_exc(g_coord,g_num,totex,ntote,12)
   call dis_exc(loads,lnf,0.1,g_coord,g_num,totex,ntote,13)
   call vec_exc(loads,lnf,0.1,0.1,g_coord,g_num,totex,ntote,14)
   if(iters==limit)exit
   deallocate(kb,exc_loads,bdylds,oldis,loads,exele)
 end do layer_number
stop
end program p610_1
```

Graphics subroutines

The graphics subroutines mentioned above require the following arguments:

`subroutine mesh_exc(g_coord,g_num,totex,ntote,ips)`

Subroutine that creates the PostScript output file `*.msh` of the undeformed mesh following excavation.

`call dis_exc(loads,lnf,ratmax,g_coord,g_num,totex,ntote,ips)`

Subroutine that creates the PostScript output file `*.dis` of the deformed mesh following excavation.

`call vec_exc(loads,lnf,ratmax,cutoff,g_coord,g_num,totex,ntote,ips)`

Subroutine that creates the PostScript output file `*.vec` of the nodal displacment vectors following excavation.

Table 3.2. Graphics routine arguments

|	
g_coord(2,nn)	nodal coordinates
g_num(8,nels)	element node numbers
ntote	number of excavated elements
totex(ntote)	excavated element numbers
ips	output channel number
loads(neq)	nodal displacements
lnf(2,nn)	active nodal freedom array
ratmax	maximum nodal displacement $\div$ maximum mesh dimension
cutoff	shortest arrow length $\div$ maximum nodal displacement

43

Results File p610_1.res

```
The total number of elements is      16
The total possible number of equations is:   96
Excavation number   1

There are      86 freedoms and nband is    29 in step      1
Increment  1 took     2 iterations to converge
Increment  2 took     2 iterations to converge
Increment  3 took     2 iterations to converge
Increment  4 took     2 iterations to converge
Increment  5 took     2 iterations to converge
The displacements are :
   29  0.7636E-05 -0.5876E-04
   61  0.0000E+00  0.1223E-03


Excavation number   2

There are      76 freedoms and nband is    29 in step      2
Increment  1 took     2 iterations to converge
Increment  2 took     2 iterations to converge
Increment  3 took     4 iterations to converge
Increment  4 took     6 iterations to converge
Increment  5 took    31 iterations to converge
The displacements are :
   29  0.8717E-04 -0.3952E-03
   61  0.0000E+00  0.2324E-03
```
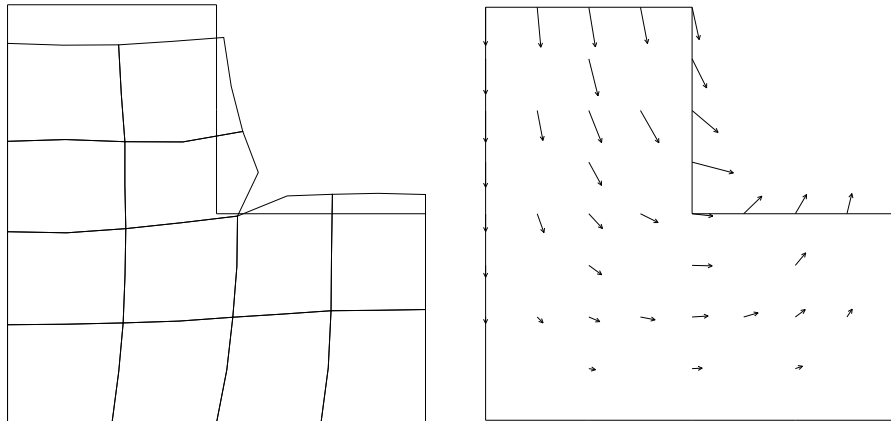

Figure 31. Deformed mesh and displacement vectors following second excavation in vertical cut analysis

.

44

Even in this rather simple problem, it is clear that the vertical displacement at the crest of the excavation (node 29) increases quite rapidly (from -0.5876E-04 to -0.3952E-03) following the second excavation of elements 10 and 14. It can also be seen that the algorithm requires a sudden increase in the number of iterations (from 6 to 31) for convergence when the fifth increment of the second excavation is applied.

The critical height of a vertical cut in undrained clay (e.g. Terzaghi and Peck 1967) is given by:

$$H_{cr} \approx \frac{c_u}{0.26 \; \gamma} \tag{14}$$

which gives $H_{cr} \approx 1.92$m, hence the finite element analysis agrees quite closely with the classical solution even with a rather crude mesh. Figure 31 shows the deformed mesh and nodal displacement vectors corresponding to the final increment of the second excavation step. The mechanism of failure clearly indicates side wall bulging combined with base heave.

3.3 Excavation in frictional soil

In this example (Calderon 2000), an excavation with a slope of 37° to the horizontal is created in a deep layer of homogeneous soil with properties, $\phi^{'} = 22^o$, $c^{'} = 40$kN/m^2 and $\gamma = 18$kN/m^3. Bishop's method indicates that the slope will reach a factor of safety of unity when the depth of the excavation reaches about 63.5m. Using Program p610_1.f90 Figure 32 shows the computed vertical displacement at the crest of the slope as a function of excavation depth. Following some heave in the initial stages due to unloading, a very sudden increase in crest displacement is apparent following the 13th excavation indicating that failure would occur with an excavated slope height in the range 60m $< H <$ 65m. Figure 33 shows the deformed mesh plot corresponging to the final excavation step.

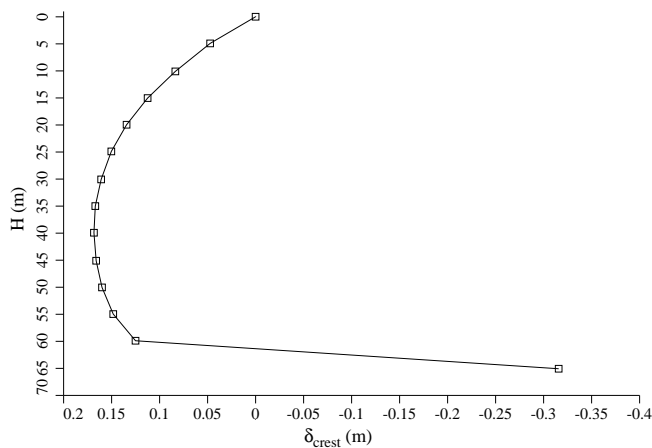**Figure 32.** Crest deformation as a function of excavation depth

.

45

Deformations have been scaled
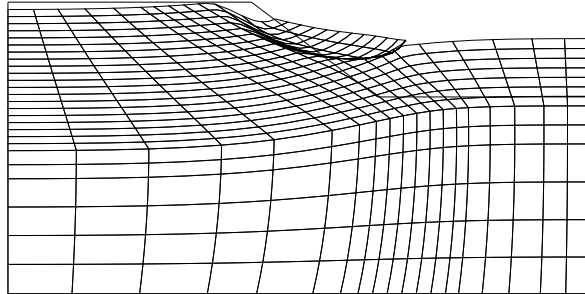**to emphasise the mechanism of failure**

Figure 33. Deformed mesh at excavated slope height of 65m

.

3.4 Excavation of a tunnel

In this example an analysis of an underground excavation is demonstrated using Program `p610_1.f90`. A 5m high horizontal "tunnel" is constructed in clay with an undrained shear strength of $c_u = 100\text{kN/m}^2$ and total unit weight of $\gamma = 20\text{kN/m}^3$. The centerline of the excavation is at a depth of 5.5m and the in-situ total stresses in the ground prior to excavation have been assumed hydrostatic. Only half the problem is analysed due to symmetry. The excavation is gradually enlarged laterally and the vertical deflection of the ground surface above the center of the excavation recorded. The roof eventually caves when the width of the tunnel reaches 10m as shown in Figures 34 and 35.
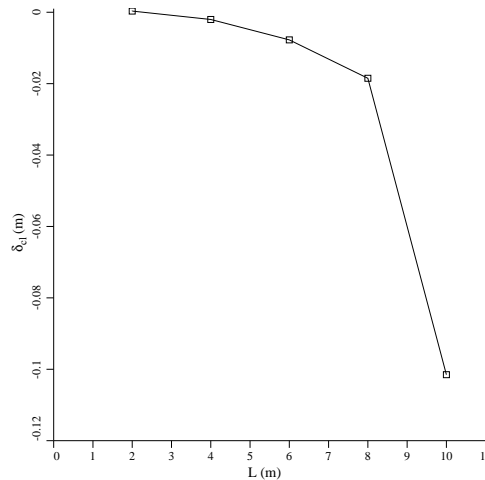

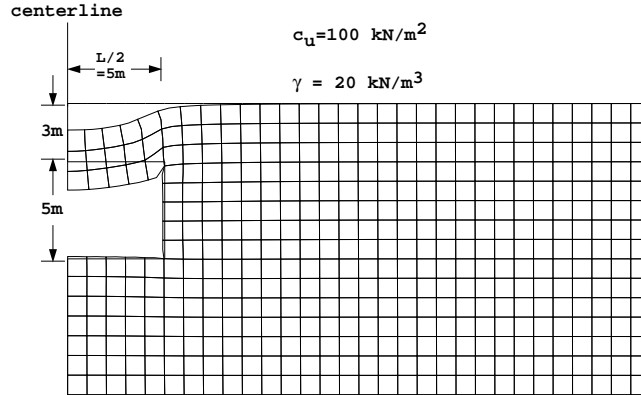**Figure 34.** Centerline ground surface deformation as a function of tunnel width

.

46

Figure 35. Deformed mesh when tunnel width reaches $L = 10$m

.

4 Bearing capacity of layered soils

Bearing capacity analysis is a more severe test of an elasto-plastic finite element code than slope stability analysis, due to the more confined nature of the problem. In part, this is due to the sensitivity of the computed values to the volume change tendency of the soil as defined by the plastic potential function or, in the case of "simple" models, the dilation angle ψ.

The volume change issue is not addressed in this section, because in the examples that follow, the soils that are modelled are "undrained clays", thus an associated Tresca failure criterion has been used implying no volume change during yielding.

4.1 A two-layer clay problem

The problem to be considered in this section is the bearing capacity of a rigid smooth strip footing resting on a two-layer clay soil foundation. A typical finite element mesh is shown in Figure 36. This problem has interested researchers for many years, initially using upper-bound limit analysis approaches (Button 1953, Brown and Meyerhof 1969, Chen 1975), and subsequently using numerical approaches (Griffiths 1982). Very recently, the problem has been revisited by Merifield *et al* 1999 using both upper *and* lower bound approaches and these solutions will form the basis of the comparisons with finite element results given in this section.

For the special case of $c_{u1} = c_{u2} = c_u$, the "Prandtl problem" is retrieved in which the ultimate bearing capacity is given by:

$$q_{ult} = (2 + \pi)c_u \tag{15}$$

If $c_{u1}/c_{u2} < 1$ then the footing is resting on soft clays overlying older, stiffer glacial tills. Alternatively, if $c_{u1}/c_{u2} > 1$, then the footing is resting on a strong surface crust
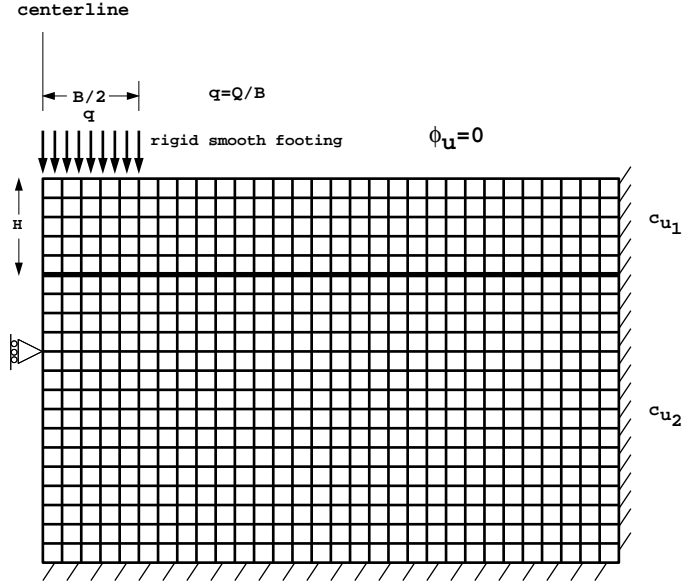
47

Figure 36. Mesh and configuration of two-layer bearing capacity problem

overlying weaker soils. The stronger crust may have been caused by dessication or weathering. One of the chief questions of interest in layered problems like this is, "How thick must the upper layer be before the influence of the lower layer becomes insignificant?"

Results have indicated that considerably more interaction occurs between the layers if the upper layer is the stronger of the two ($c_{u1}/c_{u2} > 1$). Brown and Meyerhof (1969) recorded a reduction in bearing capacity in such problems up to a depth ratio of $H/B \approx 2.5$, providing $c_{u2} < 0.2c_{u1}$. In the case of a weaker upper layer ($c_{u1}/c_{u2} < 1$), the lower soil strength was found to be immaterial for $H/B > 0.7$ and simply acted as a firm base. This seems consistent with the theoretical Prandtl mechanism which extends to a depth of $H/B = 1/\sqrt{2} = 0.707$.

4.2 Comparison of finite element and limit analysis

The program used in this study is a slightly modified version of Program 6.8 (2-d plane strain, 8-node quadrilaterals, viscoplasticity reduced integration) in the text by Smith and Griffiths (1998). The modifications mainly relate to the organisation of output, and the inclusion of graphics routines for plotting displacement vectors.

In all the analyses (Goss and Griffiths 2001), a vertical downward displacement δ_v, was applied incrementally to the footing. Nodal reactions beneath the footing were back-figured after each increment from the converged stress field (Woodward and Griffiths 1998), by assembly of the nodal forces in the elements directly beneath the footing given by:

$$Q = \sum \int_{V^e} \mathbf{B}^T \sigma dV^e \tag{16}$$

Convergence after each increment was defined as having occurred when the nodal displacements from one iteration to the next were changing by less that 0.01%. Bearing

capacity failure was deemed to have occurred when the nodal reactions levelled out to within a tolerance of 0.1%.

The shear strength of each layer of undrained clay was governed by Tresca's failure criterion defined by the dimensionless function:

$$F = \frac{(\sigma_1 - \sigma_3)}{2c_u} - 1 \tag{17}$$

Positive values of F (see Section 1.3) generated within the mesh were considered "illegal" and redistributed to neighbouring regions that still had reserves of strength.
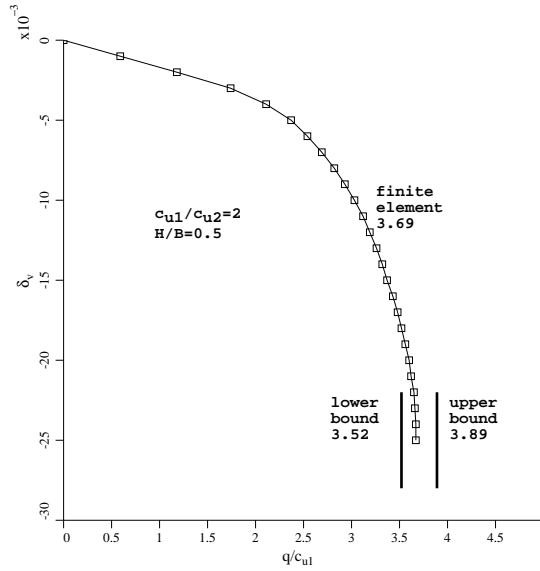

Figure 37. Plot of q/c_{u1} vs. δ_v for $c_{u1}/c_{u2} = 2$, $H/B = 0.5$

.

A typical plot of q/c_{u1} vs. δ_v is shown in Figure 37 for the case of $c_{u1}/c_{u2} = 2$ and $H/B = 0.5$. The finite element result is compared directly with the upper and lower bound results from Merifield *et al* 1999.

Defining a modified bearing capacity factor with respect to the strength of the upper soil as follows:

$$N_c^* = q_u/c_{u1} \tag{18}$$

it appears that the finite element result of $N_c^* \approx 3.69$ lies between the lower and upper bound solutions of $N_c^* \approx 3.52$ and $N_c^* \approx 3.89$ respectively.

A more complete set of finite element computed N_c^* values for a range of parameters is shown in Tables 4.1 and 4.2, together with upper and lower bound solutions and F_{max}, the largest value of the failure function as given by equation (17) at any point within the mesh at convergence. It should be noted that "perfect convergence" would imply

49

$F_{max} = 0$ at all Gauss points. A graphical solution to selected results in the table is given in Figure 38.

Table 4.1. Computed values of N_c^*, $H/B < 1$

H/B	c_{u1}/c_{u2}	Lower bound	FE	Upper bound	F_{max}
	0.20	5.44	5.81	5.89	0.0254
	0.25	5.44	5.79	5.89	0.0201
	0.33	5.44	5.78	5.89	0.0154
	0.40	5.44	5.77	5.89	0.0118
	0.50	5.44	5.76	5.89	0.0076
	0.57	5.44	5.75	5.89	0.0062
	0.66	5.42	5.75	5.89	0.0052
	0.80	5.30	5.63	5.71	0.0031
	1.00	4.86	5.11	5.32	0.0014
0.2	1.25	4.06	4.34	4.57	0.0024
	1.50	3.57	3.80	4.02	0.0017
	1.75	3.19	3.40	3.59	0.0018
	2.00	2.90	3.08	3.24	0.0015
	2.50	2.46	2.61	2.77	0.0012
	3.00	2.15	2.28	2.44	0.0008
	3.50	1.93	2.03	2.19	0.0006
	4.00	1.75	1.82	2.00	0.0006
	5.00	1.48	1.51	1.73	0.0006
	0.20	4.86	5.14	5.31	0.0110
	0.25	4.86	5.14	5.31	0.0093
	0.33	4.86	5.14	5.31	0.0070
	0.40	4.86	5.14	5.31	0.0059
	0.50	4.86	5.14	5.31	0.0040
	0.57	4.86	5.14	5.31	0.0034
	0.66	4.86	5.14	5.31	0.0029
	0.80	4.86	5.14	5.31	0.0021
	1.00	4.86	5.11	5.32	0.0015
0.5	1.25	4.42	4.66	4.94	0.0019
	1.50	4.07	4.27	4.48	0.0024
	1.75	3.77	3.95	4.16	0.0024
	2.00	3.52	3.69	3.89	0.0019
	2.50	3.13	3.27	3.47	0.0017
	3.00	2.84	2.96	3.16	0.0015
	3.50	2.62	2.71	2.93	0.0013
	4.00	2.44	2.50	2.74	0.0011
	5.00	2.16	2.15	2.44	0.0008

Table 4.2. Computed values of N_c^*, $H/B \geq 1$

H/B	c_{u1}/c_{u2}	Lower bound	FE	Upper bound	F_{max}
	0.20	4.94	5.11	5.32	0.0074
	0.25	4.94	5.11	5.30	0.0058
	0.33	4.94	5.11	5.30	0.0044
	0.40	4.94	5.11	5.30	0.0037
	0.50	4.94	5.11	5.30	0.0026
	0.57	4.94	5.11	5.30	0.0023
	0.66	4.94	5.11	5.30	0.0020
	0.80	4.94	5.11	5.30	0.0016
	1.00	4.94	5.11	5.30	0.0014
1.0	1.25	4.87	5.11	5.30	0.0011
	1.50	4.77	4.97	5.18	0.0010
	1.75	4.60	4.78	5.00	0.0009
	2.00	4.44	4.61	4.82	0.0010
	2.50	4.14	4.33	4.50	0.0010
	3.00	3.89	4.12	4.24	0.0007
	3.50	3.69	3.95	4.02	0.0006
	4.00	3.46	3.81	3.83	0.0006
	5.00	3.10	3.58	3.54	0.0005
	0.20	4.94	5.11	5.30	0.0070
	0.25	4.94	5.11	5.30	0.0058
	0.33	4.94	5.11	5.30	0.0041
	0.40	4.94	5.11	5.30	0.0034
	0.50	4.94	5.11	5.30	0.0029
	0.57	4.94	5.11	5.30	0.0025
	0.66	4.94	5.11	5.30	0.0021
	0.80	4.94	5.11	5.30	0.0017
	1.00	4.94	5.11	5.32	0.0013
1.5	1.25	4.87	5.11	5.27	0.0024
	1.50	4.87	5.11	5.31	0.0019
	1.75	4.87	5.11	5.31	0.0017
	2.00	4.87	5.11	5.31	0.0014
	2.50	4.84	5.07	5.32	0.0014
	3.00	4.69	4.94	5.15	0.0014
	3.50	4.46	4.79	4.98	0.0012
	4.00	4.24	4.69	4.84	0.0011
	5.00	3.89	4.50	4.56	0.0009

The upper and lower bounds bracket the displacement finite element results, the one exception being when $H/B = 1$ and $c_{u1}/c_{u2} = 5$, where the upper bound solution appears to drift slightly below the finite element result.

The reason for this discrepancy is unclear, however the Tables indicate consistently small values of F_{max}, indicating a high level of convergence and accuracy in the finite element results.
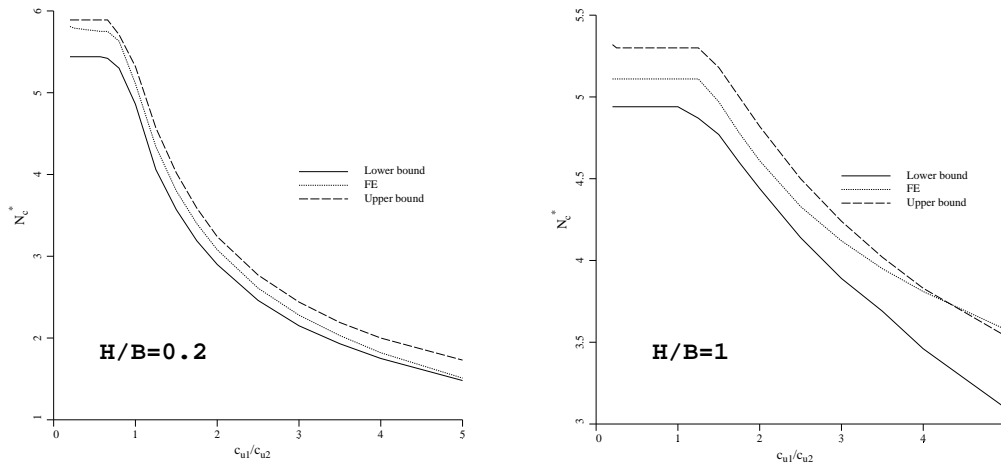
51

Figure 38. Comparison of finite element with lower and upper bound solutions
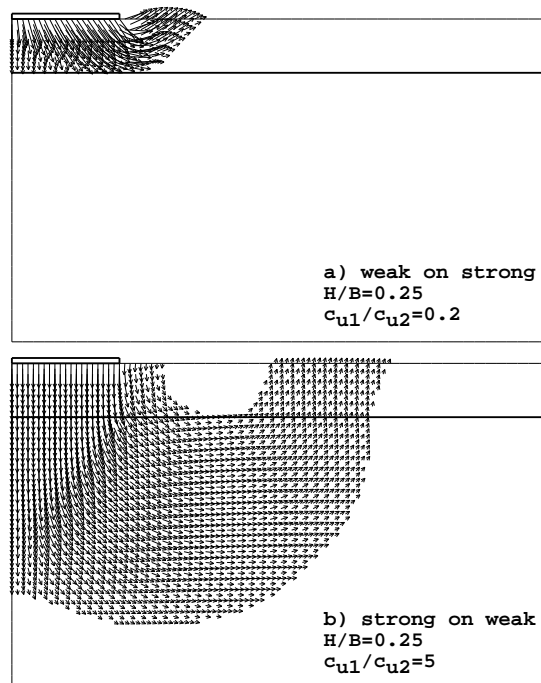

Figure 39. Typical vector plots at failure. a) weak on strong, b) strong on weak.

Figure 39 shows typical nodal displacement patterns from the displacement finite element analyses at failure for the cases of "weak on strong" and "strong on weak". The contrasting nature of the failure mechanisms in each case is clearly indicated.

In summary, while limit analysis can be useful for providing validation checks, the elasto-plastic finite element method is a more powerful and practically useful method for computing bearing capacity. It has been shown that in a single analysis, the method can be relied upon to give robust and accurate solutions to a wide range of geotechnical "failure" problems.

5 A Probabilistic Approach to Bearing Capacity using Finite Elements

The final section of this report extends the elasto-plastic finite element method described above to investigate the bearing capacity of clays with spatially randomly varying shear strength. The methodology is essentially the same as that described in Section 2 for slope stability. The objective of the investigation is to determine the extent to which variance and spatial correlation of the soil's undrained shear strength impacts on the statistics of the bearing capacity. Throughout this section, bearing capacity results are expressed in terms of the bearing capacity factor, N_c, in relation to the *mean* undrained strength. For low coefficients of variation $(C.O.V._{c_u})$ of shear strength, the expected value of the bearing capacity factor tends to the Prandtl solution of $N_c = 5.14$. For higher values of $(C.O.V._{c_u})$ however, the expected value of the bearing capacity factor falls quite steeply. As in the slope stability studies, the spatial correlation length is shown to be an important parameter which should not be ignored. The results of Monte-Carlo simulations on this nonlinear problem are presented in the form of histograms, which enable the interpretation to be expressed in a probabilistic context. Results obtained in this study help to explain why bearing capacity calculations require relatively high factors of safety compared to other branches of geotechnical design.

5.1 Introduction

This section presents results obtained using a program developed by the authors (Griffiths and Fenton 2001) which merges nonlinear elasto-plastic finite element analysis such as described in the previous section, with random field theory. The program computes the bearing capacity of a smooth rigid strip footing (plane strain) at the surface of a undrained clay soil with a shear strength c_u $(\phi_u = 0)$ defined by a spatially varying random field.

Rather than deal with the actual bearing capacity, this study focuses on the dimensionless bearing capacity factor N_c defined:

$$N_c = q_f / \mu_{c_u} \tag{19}$$

where q_f is the bearing capacity and μ_{c_u} is the mean undrained shear strength of the soil beneath the footing. For a homogeneous soil with a constant undrained shear strength, N_c is given by the Prandtl solution (eqn. 15) and equals $2 + \pi$ or 5.14. For soils with a

variable shear strength, the bearing capacity factor will be defined with respect to the *mean* undrained shear strength.

In this study, the variability of the undrained shear strength is lognormal, and defined by the same three statistical parameters shown in Table 2.1. In the parametric studies that follow, the mean strength (μ_{c_u}) has been held constant at 100 kN/m^2, while the coefficient of variation $(C.O.V._{c_u})$ and spatial correlation length $(\Theta_{c_u} = \theta_{\ln c_u}/B)$, non-dimensionalised with respect to the footing width B, are varied systematically.

For each set of assumed statistical properties given by $C.O.V._{c_u}$ and Θ_{c_u}, Monte-Carlo simulations have been performed. These typically involve 1000 repetitions or "realizations" of the shear strength random field and the subsequent finite element analysis of bearing capacity. This means that each realization, while having the same underlying statistics, leads to a quite different spatial pattern of shear strength values beneath the footing. Each realization, therefore, leads to a different value of the bearing capacity and, after normalization by the *mean* undrained shear strength, a different value of the bearing capacity factor,

$$N_{c_i} = q_{f_i}/\mu_{c_u}, \qquad i = 1, 2, ..., n_{sim} \tag{20}$$

IN this study, $n_{sim} = 1000$, and once the bearing capacity factors from all the realisations have been accumulated, they in turn can be subjected to statistical analysis. Estimated (sample) mean bearing capacities will a have standard error ($\pm$ one standard deviation) equal to the sample standard deviation times $1/\sqrt{n} = 1/\sqrt{1000} = 0.032$, or about 3% of the sample standard deviation. Similarly, the sample variance will have standard error of about 0.04 times the sample variance. This means that estimated quantities will generally be within about 5% of the true quantities, statistically speaking.

Of particular interest in the present study, is the *probability* that the actual bearing capacity factor, N_c, as defined in equation (20), will be *less* than the Prandtl value of 5.14 that would be obtained assuming a homogeneous soil with the undrained shear strength everywhere equal to the mean value μ_{c_u}.

5.2   Review of the lognormal distribution

As in the Slope Stability analyses of Section 2, a lognormal distribution for the undrained shear strength c_u has been adopted, meaning that $\ln c_u$ is normally distributed. If the mean and standard deviation of the undrained shear strength are μ_{c_u} and σ_{c_u} respectively, then the standard deviation and mean of the underlying normal distribution of $\ln c_u$ are given by:

$$\sigma_{\ln c_u} = \sqrt{\ln\left\{1 + \left(\frac{\sigma_{c_u}}{\mu_{c_u}}\right)^2\right\}} \tag{21}$$

$$\mu_{\ln c_u} = \ln \mu_{c_u} - \frac{1}{2}\sigma_{\ln c_u}^2 \tag{22}$$

and the probability density function of the lognormal distribution by:

$$f(c_u) = \frac{1}{c_u \ \sigma_{\ln c_u} \ \sqrt{2\pi}} \ \exp\left\{ -\frac{1}{2} \left(\frac{\ln c_u - \mu_{\ln c_u}}{\sigma_{\ln c_u}} \right)^2 \right\} \tag{23}$$
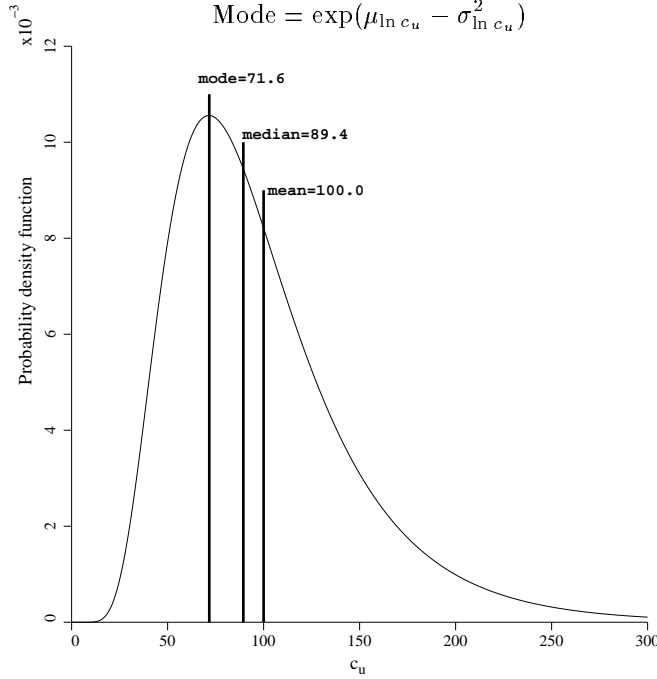
The properties of the lognormal distribution can therefore be summarized as:

$$\mu_{c_u} = \exp\left(\mu_{\ln c_u} + \frac{1}{2}\sigma_{\ln c_u}^2 \right) \tag{24}$$

$$\sigma_{c_u} = \mu_{c_u} \sqrt{\exp(\sigma_{\ln c_u}^2) - 1} \tag{25}$$

$$\text{Median} = \exp(\mu_{\ln c_u}) \tag{26}$$

$$\text{Mode} = \exp(\mu_{\ln c_u} - \sigma_{\ln c_u}^2) \tag{27}$$

Figure 40. Typical lognormal distribution of undrained shear strength with a mean of 100 and standard deviation of 50 ($C.O.V._{c_u} = 0.5$). All units are in kN/m^2.

A typical lognormal distribution based on equation (23) with mean $\mu_{c_u} = 100$ kN/m^2 and standard deviation $\sigma_{c_u} = 50$ kN/m^2 ($C.O.V._{c_u} = 0.5$) is shown in Figure 40. From equations (21) and (22) it is easily shown that the underlying "normal" statistics are given by $\sigma_{\ln c_u} = 0.472$ and $\mu_{\ln c_u} = 4.494$. Highlighted also on the figure are the median and mode of the distribution, which can be shown from equations (26) and (27) to equal, respectively, 89.4 kN/m^2 and 71.6 kN/m^2. The skewed nature of the lognormal distribution always results in the mode, median and mean being in the sequence indicated. In a lognormal distribution, the median is always smaller than the mean, and this will have

55

implications for the probabilistic interpretation of the bearing capacity results described later in this section.

Use of the lognormal distribution, as opposed to the more familiar normal distribution, or even some other more complex distribution, is based on the following arguments: Firstly, there is a lack of exhaustive field data that would be necessary to conclusively support one kind of distribution over another. However, there is some evidence from the field to support the lognormal distribution for some soil properties (see e.g. Hoeksema and Kitanidis 1985, and Sudicky 1986). Use of the lognormal distribution is also based on the simplicity and familiarity of its two-parameters description. Secondly, and perhaps most importantly from a physical standpoint, the lognormal distribution is strictly non-negative, unlike the normal distribution, and so there is no possibility of generating properties with meaningless negative values, particularly in the extremes of the distribution (which may be important from a reliability standpoint). It might also be noted that a lognormal distribution looks quite similar to a normal distribution for low values of the $C.O.V.$.

Lee *et al* (1983) comment that the "normal or lognormal distributions are adequate for the large majority of geotechnical data" however Harr (1987) finds the unbounded nature of the upper end of the lognormal distribution objectionable. The potential for the lognormal distribution to generate very high property values (albeit with a low probability) is not considered a serious flaw, especially in a study involving the shear strength of heterogeneous soil that is spatially distributed (what is the shear strength of a point that happens to fall inside a boulder of granite?). It is certainly possible that a soil deposit will contain occasional inclusions of very strongly cemented material.
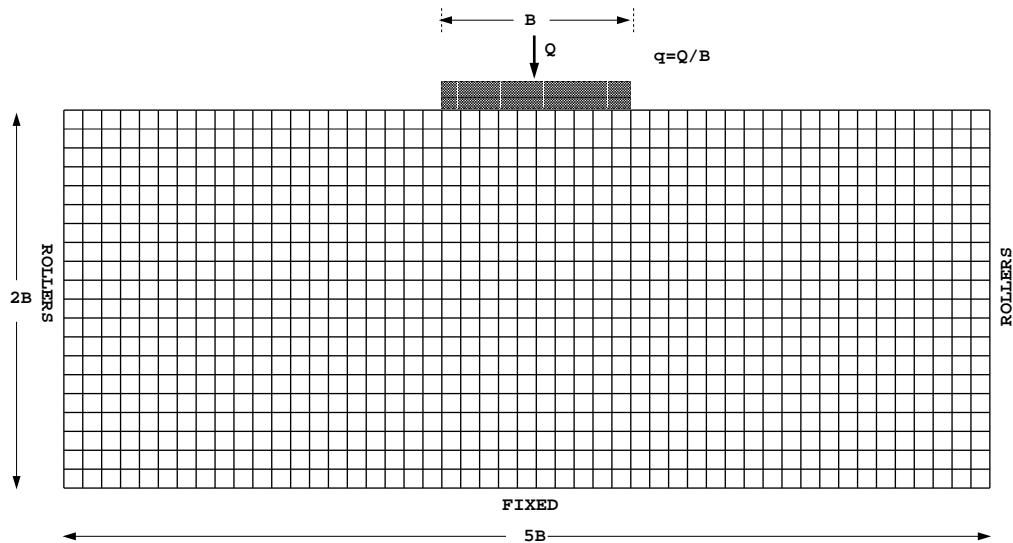
5.3   Brief description of FE method used

Figure 41. Mesh used in probabilistic bearing capacity analyses (units in m).

A typical mesh is shown in Figure 41 consisting of 1000 elements, with 50 columns and 20 rows. Each element is square, and the strip footing has a width of 10 elements. The bearing capacity analyses use essentially the same program as described in the previous section for a two-layer soil incorporating a Tresca failure criterion.

The finite element model incorporates three parameters; Young's modulus (E), Poisson's ratio (ν) and the undrained shear strength (c_u). The methodology allows for random distributions of all three parameters, however in the present study, E and ν are held constant while c_u is randomized.

At the ith realisation of the Monte-Carlo process, the footing is incrementally displaced vertically (δ_v) into the soil and the sum of the nodal reactions (Q_i) back-figured from the converged stress state. When the sum of the nodal reactions levels out to within a quite strict tolerance (see Section 4.2), "failure" is said to have occurred and the sum of the nodal reactions divided by the footing area is the "bearing capacity" ($q_{f_i} = Q_{f_i}/B$) of that particular realisation.

5.4 Brief description of the random field model

The undrained shear strength is obtained through the transformation

$$c_{u_i} = \exp\{\mu_{\ln c_u} + \sigma_{\ln c_u} g_i\} \tag{28}$$

in which c_{u_i} is the undrained shear strength assigned to the ith element, g_i is the local average of a standard Gaussian random field, g, over the domain of the ith element, and $\mu_{\ln c_u}$ and $\sigma_{\ln c_u}$ are the mean and standard deviation of the logarithm of c_u (obtained from the "point" mean and standard deviation μ_{c_u} and σ_{c_u} after local averaging).

The LAS technique (Fenton 1990, Fenton and Vanmarcke 1990) generates realizations of the local averages g_i which are derived from the random field g having zero mean, unit variance, and a spatial correlation length, $\theta_{\ln c_u}$. As the spatial correlation length tends to infinity, g_i becomes equal to g_j for all elements i and j – that is the field of shear strengths tends to become uniform on each realization. At the other extreme, as the spatial correlation length tends to zero, g_i and g_j become independent for all $i \neq j$ – the soil's undrained shear strength changes rapidly from point to point. In the present study, a Markovian spatial correlation function was used, of the form:

$$\rho(|\tau|) = \exp\left\{-\frac{2}{\theta_{\ln c_u}} |\tau|\right\} \tag{29}$$

where ρ is the correlation coefficient between the logarithm of the undrained strength values at any two point separated by a distance τ in a random field with spatial correlation length $\theta_{\ln c_u}$.

In the two-dimensional analyses presented in this paper, the spatial correlation lengths in the vertical and horizontal directions are taken to be equal (isotropic) for simplicity. Fenton (1999) examined CPT data in relation to random field modeling, however the actual spatial correlation structure of soil deposits is not usually well known, especially in the horizontal direction (see e.g. DeGroot and Baecher 1993, de Marsily 1985, Asaoka

and Grivas 1982). In this paper therefore, a parametric approach has been employed to study the influence of $\theta_{\ln c_u}$.

The plane strain model used herein implies that the out-of-plane spatial correlation length is infinite, thus soil properties are constant in this direction. This is clearly a deficiency. However, previous studies by the authors (Griffiths and Fenton 1997) involving seepage through two- and three-dimensional random fields have indicated that the difference may not be very great. The role of the third dimension is an area of ongoing research by the authors.

A local averaging process has been included in the formulation to take full account of the level of mesh discretization, and the size of the finite elements onto which the random field is to be mapped. Local averaging preserves the mean, but reduces the standard deviation of the underlying normal field to a "target" value . The amount by which the standard deviation is reduced, depends on the size of the elements and the nature of the spatial correlation function governing the field. More specifically, there is a function called the "variance function", which can be derived from the correlation function, which governs the rate at which the standard deviation drops as the averaging domain grows larger. The interested reader is referred to Vanmarcke (1984) for a detailed description of this formulation.

Although the mean of the underlying Gaussian field is unaltered by local averaging, equations (24) and (25) indicate that since both the mean *and* standard deviation of the lognormal field are functions of $\sigma_{\ln c_u}$ they will *both* be reduced by the local averaging process. Thus the coarser the mesh, the greater the reduction in the "target" statistics from their nominal "point" values. This local averaging approach is fully implemented in this study, and removes any "mesh effects" that might otherwise be present. It might also be commented that this approach is quite consistent with the philosophy of the finite element method in which finer meshes resolve the finer variations in the stress and material property fields.

5.5   Parametric studies

Analyses were performed using the mesh of Figure 41 with the input parameters in the following ranges:

$$0.125 \leq \quad \Theta_{c_u} \quad < \infty \tag{30}$$
$$0.125 \leq C.O.V._{c_u} \leq 4$$

To indicate the nature of the different solutions obtained at each realisation of the Monte-Carlo process, load/deformation results for 10 typical realisations of the footing analysis are shown in Figure 42 for the case when $\Theta_{c_u} = 1$ and $C.O.V._{c_u} = 1$. The average stress q under the footing has been non-dimensionalised by dividing it by the mean undrained shear strength μ_{c_u}. The reader should bear in mind the Prandtl solution of 5.14 when viewing this figure. It is clear that a majority of the curves flatten out at bearing capacity values below the Prandtl solution. This trend will be confirmed in all the results shown in this paper.
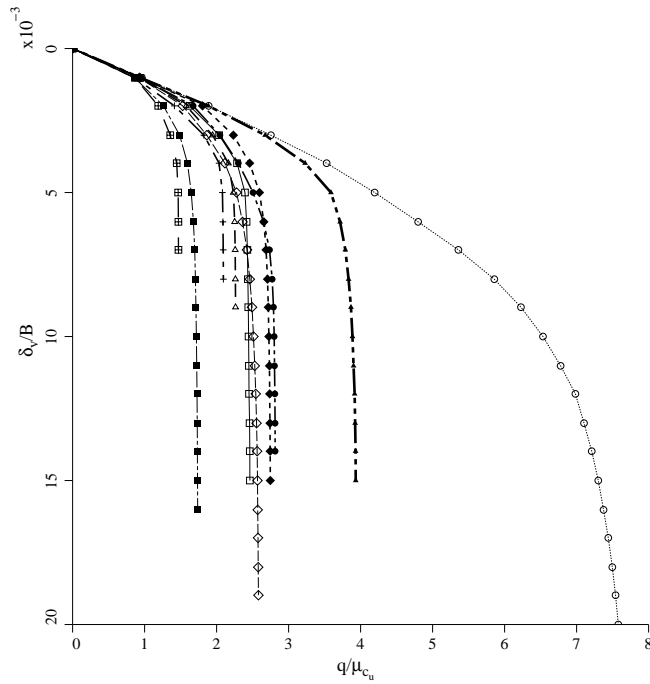
Figure 42. Typical load/deformation curves corresponding to different realizations in the bearing capacity analysis of an undrained clay with $\Theta_{c_u} = 1$ and $C.O.V._{c_u} = 1$.

Figure 43 shows a typical deformed mesh at failure with a superimposed greyscale corresponding to $\Theta_{c_u} = 1$, in which lighter regions indicate stronger soil and darker regions indicate weaker soil. In this case the dark zones and the light zones are roughly the width of the footing itself, and it appears that the weak (dark) region near the ground surface to the right of the footing has triggered a quite non-symmetric failure mechanism. The shape of the non-symmetric mechanism is emphasised further by the plot of displacement vectors for the same realisation shown in Figure 44.
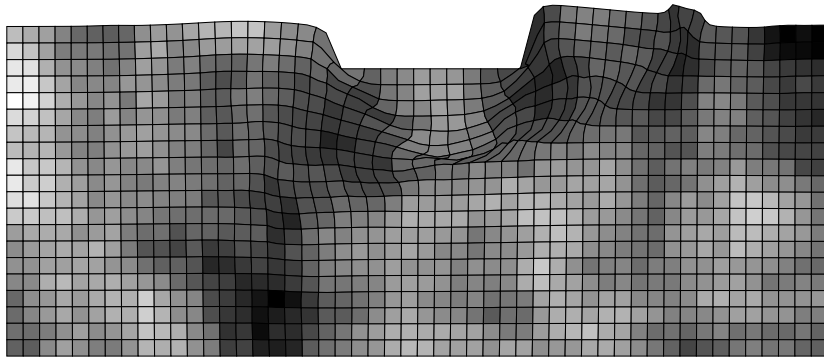

Figure 43. Typical deformed mesh and greyscale at failure with $\Theta_{c_u} = 1$. The darker regions indicate weaker soil.

59
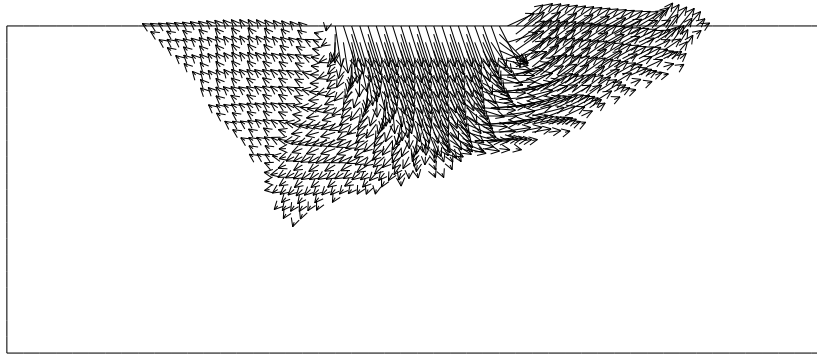
Figure 44. Displacement vectors at failure for the same case shown in Figure 43. The non-symmetric shape of the failure mechanism is clearly visible.

For each combination of Θ_{c_u} and $C.O.V._{c_u}$, $n_{sim} = 1000$ realisations of the Monte-Carlo process were performed, and the estimated mean (m_{N_c}) and standard deviation (s_{N_c}) of the resulting 1000 bearing capacity factors from equation (20) computed.

Figure 45a shows how the estimated mean bearing capacity factor m_{N_c} varies with Θ_{c_u} and $C.O.V._{c_u}$. The plot confirms that for low values of $C.O.V._{c_u}$, m_{N_c} tends to the deterministic Prandtl value of 5.14. For higher values of $C.O.V._{c_u}$ however, the mean bearing capacity factor falls steeply, especially for lower values of Θ_{c_u}. For example, in a highly variable case where $\Theta_{c_u} = 0.5$ and $C.O.V._{c_u} = 4$, the predicted m_{N_c} value is less than unity – over five times smaller than the Prandtl value! For the recommended upper limit of $C.O.V._{c_u} = 0.5$ suggested by Lee et al (1983) and others, the m_{N_c} value is closer to 4, corresponding to a more modest reduction of 20%.
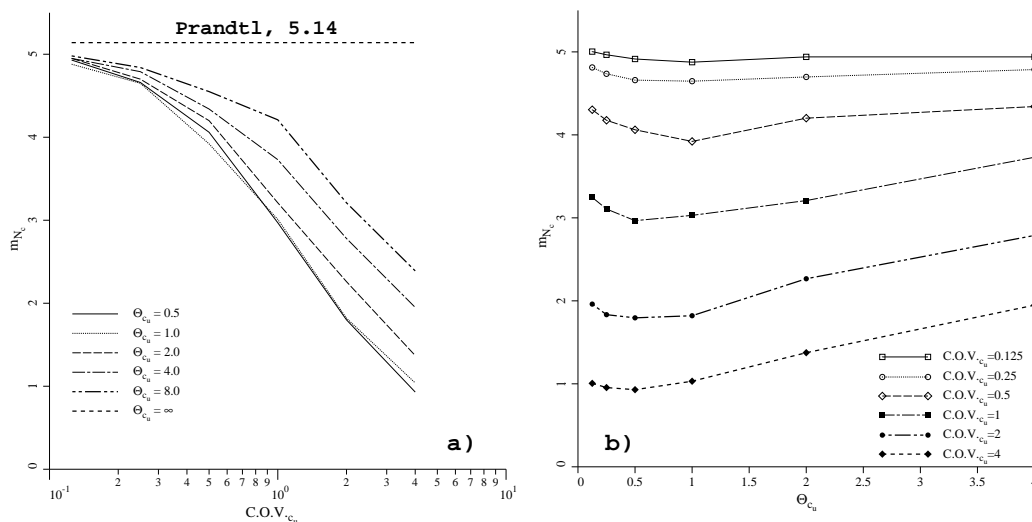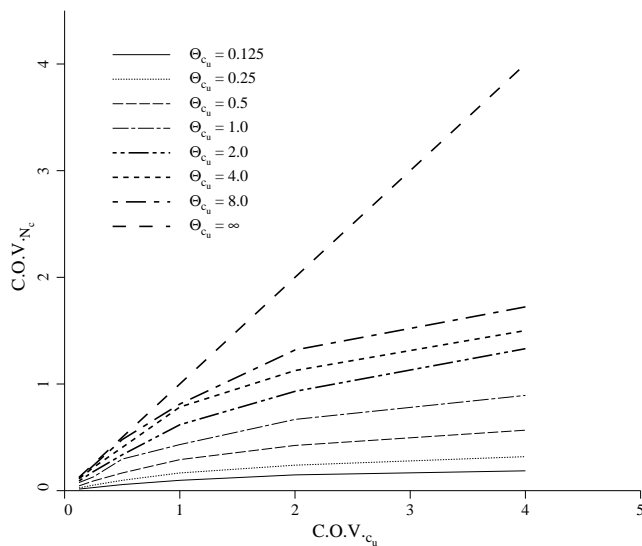

Figure 45. Estimated mean bearing capacity factor m_{N_c} as a function of undrained shear strength statistics, Θ_{c_u} and $C.O.V._{c_u}$.

What this implies from a design standpoint, is that the bearing capacity of a heterogeneous soil, will on average be *less* than the Prandtl solution that would be predicted assuming the soil is homogeneous with its strength given by the mean value. The influence of Θ_{c_u} is also pronounced, with the greatest reduction from the Prandtl solution being observed with values around $\Theta_{c_u} \approx 0.5$. As the value of Θ_{c_u} is reduced further towards zero, there is evidence of a gradual increase in the value of m_{N_c} as shown in Figure 45b. From a theoretical point of view, it could be speculated that as Θ_{c_u} becomes vanishingly small, the mean bearing capacity factor will continue to increase towards the deterministic Prandtl solution of 5.14. The explanation lies in the fact that as the spatial correlation length decreases, the weakest path becomes increasingly tortuous and its length correspondingly longer. As a result, the weakest path starts to look for shorter routes cutting through higher strength material. In the limit, as $\Theta_{c_u} \to 0$, it is expected that the optimum failure path will be the same as in a uniform material with strength equal to the mean value, hence returning to the deterministic Prandtl solution.

Also included on Figure 45a is a horizontal line corresponding to the analytical solution that would be obtained for $\Theta_{c_u} = \infty$. This hypothetical case implies that each realisation of the Monte-Carlo process involves an essentially homogeneous soil, albeit with strength varying only from one realisation to the next. In this case, the distribution of q_f will be statistically similar to the underlying distribution of c_u but magnified by 5.14. The mean bearing capacity will therefore be given by:

$$\mu_{q_f} = 5.14\mu_{c_u} \qquad (31)$$

hence $\mu_{N_c} = 5.14$ for all $C.O.V._{c_u}$.

Figure 46. Estimated coefficient of variation of the bearing capacity factor $C.O.V._{N_c} = s_{N_c}/m_{N_c}$ as a function of undrained shear strength statistics, Θ_{c_u} and $C.O.V._{c_u}$.

Figure 46 shows the influence of Θ_{c_u} and $C.O.V._{c_u}$ on the estimated coefficient of variation of the bearing capacity factor, $C.O.V._{N_c} = s_{N_c}/m_{N_c}$. The plots indicate that $C.O.V._{N_c}$ is positively correlated with both $C.O.V._{c_u}$ and Θ_{c_u}. This figure also indicates that the correlation length, Θ_{c_u}, has a significant influence on $C.O.V._{N_c}$. For small correlation lengths, $C.O.V._{N_c}$ is small and rather insensitive to $C.O.V._{c_u}$, however for higher correlation lengths, $C.O.V._{N_c}$ increases quite consistently until it reaches the limiting maximum value corresponding to $\Theta_{c_u} = \infty$, defined by the straight line where $C.O.V._{N_c} = C.O.V._{c_u}$.

5.6 Probabilistic interpretation

Following Monte-Carlo simulations for each parametric combination of input parameters (Θ_{c_u} and $C.O.V._{c_u}$), the suite of computed bearing capacity factor values from equation (20) was plotted in the form of a histogram, and a "best-fit" lognormal distribution superimposed. An example of such a plot is shown in Figure 47 for the case where $\Theta_{c_u} = 2$ and $C.O.V._{c_u} = 1$.
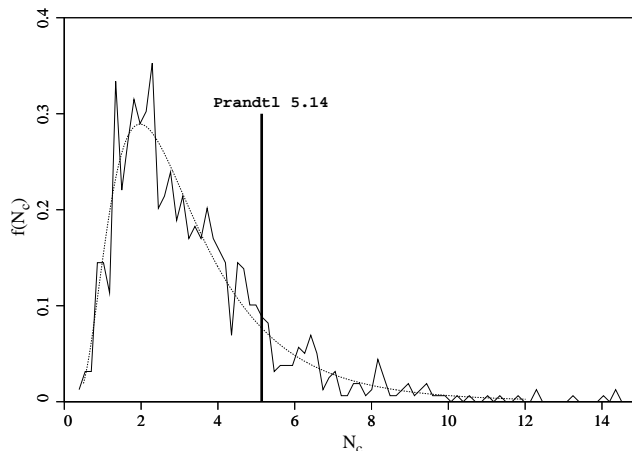
Figure 47. Histogram and lognormal fit for the computed bearing capacity factors when $\Theta_{c_u} = 2$ and $C.O.V._{c_u} = 1$. The lognormal function has the properties $m_{N_c} = 3.31$ and $s_{N_c} = 2.08$.

Since the lognormal fit has been normalized to enclose an area of unity, areas under the curve can be directly related to probabilities. From a practical viewpoint it would be of interest to estimate the probability of "design failure", defined here as occurring when the computed bearing capacity is less than the Prandtl value based on the mean strength, i.e.

$$\text{"Design failure" if } q_f < 5.14\mu_{c_u} \tag{32}$$

Let this probability be $p(N_c < 5.14)$, hence from the properties of the underlying normal distribution we get:

$$p(N_c < 5.14) = \Phi\left(\frac{\ln 5.14 - m_{\ln N_c}}{s_{\ln N_c}}\right) \tag{33}$$

where Φ is the cumulative normal function.

For the particular case shown in Figure 47, the fitted lognormal distribution has the properties $m_{N_c} = 3.31$ and $s_{N_c} = 2.08$, hence from equations (21) and (22) the underlying normal distribution is defined by $m_{\ln N_c} = 1.03$ and $s_{\ln N_c} = 0.58$. Equation (33) therefore, gives $p(N_c < 5.14) = 0.85$, indicating an 85% probability that the actual bearing capacity will be less than the Prandtl value.

Figure 48 gives a summary of $p(N_c < 5.14)$ for a range of values of Θ_{c_u} and $C.O.V._{c_u}$. The figure indicates a wide spread of probability values with respect to Θ_{c_u}, with the highest probabilities corresponding to the lowest values of Θ_{c_u}. For example, a soil with $C.O.V._{c_u} = 0.5$, exhibits a range of $0.59 < p(N_c < 5.14) < 0.95$, with the low and high values corresponding respectively to $\Theta_{c_u} = \infty$ and $\Theta_{c_u} = 0.5$.
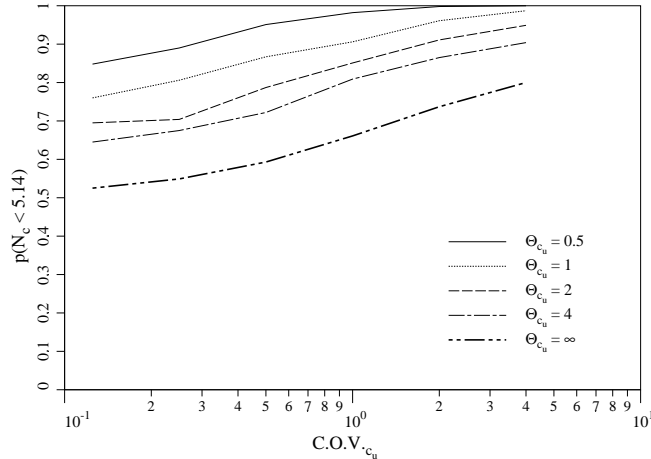
Figure 48. Graph showing the probability $p(N_c < 5.14)$ that the bearing capacity factor will be lower than the Prandtl solution based on the mean strength.

The influence of $C.O.V._{c_u}$ on the probability is also significant. Theoretically, as $C.O.V._{c_u} \rightarrow 0$, the probability $p(N_c < 5.14) \rightarrow 0.5$, irrespective of the value of Θ_{c_u}. The results in Figure 48 indicate that this convergence occurs faster for higher values of Θ_{c_u} than for lower values. It would appear that low values of Θ_{c_u} permit such widely scattered weak elements, that the probability of the actual bearing capacity lying below the Prandtl value remains high, even for low $C.O.V._{c_u}$ values. This general trend is to be expected however, because for low $C.O.V._{c_u}$ values, the distribution of bearing capacity factors becomes "bunched up" and "centered" on 5.14, giving an almost equal chance of the computed bearing capacity factor lying on either side of the Prandtl solution.

As $C.O.V._{c_u}$ is increased, the probability $p(N_c < 5.14)$ also increases. For example, when $\Theta_{c_u} = 0.5$ and $C.O.V._{c_u} = 0.5$, $p(N_c < 5.14) = 0.95$ indicating a 95% probability that the actual bearing capacity will be lower than the Prandtl solution.

The result corresponding to the limiting case of $\Theta_{c_u} = \infty$ is also indicated in Figure 48. As discussed previously, the distribution of q_f in this case is statistically similar to the underlying distribution of c_u and the required probability $p(N_c < 5.14)$, simply equals the area under the probability density function to the left of the mean. For a lognormal distribution, this probability is always greater than 0.5 and given by:

$$p(N_c < 5.14) = \Phi(0.5\, \sigma_{\ln c_u}) \tag{34}$$

thus from equation (21),

$$p(N_c < 5.14) = \Phi(0.5\, \sqrt{\ln(1 + C.O.V._{c_u}^2)}\,) \tag{35}$$

Figure 48 indicates that the expected bearing capacity of a strip footing on an undrained clay with variable shear strength defined by a lognormal distribution, will *always* be lower than the Prandtl value based on the mean strength. It could be argued, however, that this interpretation gives an over-pessimistic impression of the role of soil strength variability by not taking account of the variance of the computed bearing capacity distribution. Even an essentially deterministic analysis with a very small shear strength variance would suggest a $> 50\%$ probability that the bearing capacity would lie below the Prandtl value.
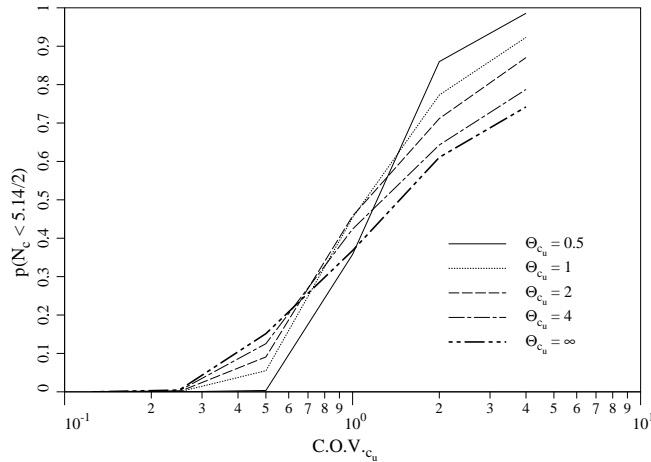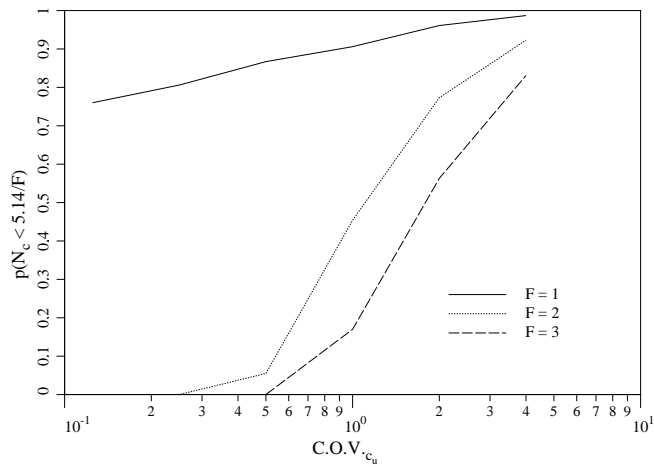

Figure 49. Graph showing the probability $p(N_c < 5.14/2)$ that the bearing capacity factor will be lower than the Prandtl solution based on the mean strength incorporating a Factor of Safety $F = 2$.

In order to remove this anomaly, the results have been reinterpreted in Figures 49 and 50 to compare the computed bearing capacity factor with the Prandtl solution after it has been reduced by a factor F. The factor F is equivalent to a "Factor of Safety" applied to the deterministic bearing capacity based on mean strength. The probability of "design failure" as measured by $p(N_c < 5.14/F)$ is now greatly reduced, giving a more reassuring result from a design viewpoint. For example, from Figure 49 in which $F = 2$,

64
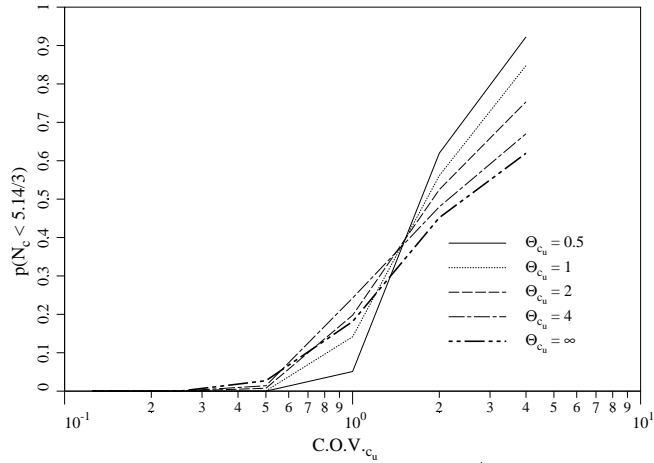
Figure 50. Graph showing the probability $p(N_c < 5.14/3)$ that the bearing capacity factor will be lower than the Prandtl solution based on the mean strength incorporating a Factor of Safety $F = 3$.


Figure 51. Graph showing the probability $p(N_c < 5.14/F)$ that the bearing capacity factor will be lower than the Prandtl solution based on the mean strength for three different Factors of Safety F for a soil with $\Theta_{c_u} = 1$.

the probability of "design failure" for a soil with $\Theta_{c_u} = 1$ and $C.O.V._{c_u} = 0.5$, is about 6%. This probability is essentially reduced to zero for the same soil, by increasing the factor to $F = 3$, as shown in Figure 50.

Figure 51 shows directly how F affects the probability of design failure for a range of $C.O.V._{c_u}$ in a soil where the correlation length is held constant at $\Theta_{c_u} = 1$. The results indicates that quite high factors of safety are required to reduce the probability of "design failure" to "acceptable" levels. Figures 50 and 51 both suggest that for a soil with $C.O.V._{c_u} = 0.5$ and $\Theta_{c_u} = 1$, a Factor of Safety of at least 3 is needed to essentially eliminate all probability of design failure. This is consistent with geotechnical engineering practice, where a factor of safety of at least 3 (e.g. Lambe and Whitman 1969) is considered necessary to protect against general shear failure.

A further interpretation of the probability of design failure is shown in Figures 52 where a direct comparison is given between the probability of "design failure" $p(N_c < 5.14/F)$ and the Factor of Safety F for a range of Θ_{c_u} and $C.O.V._{c_u}$ values.
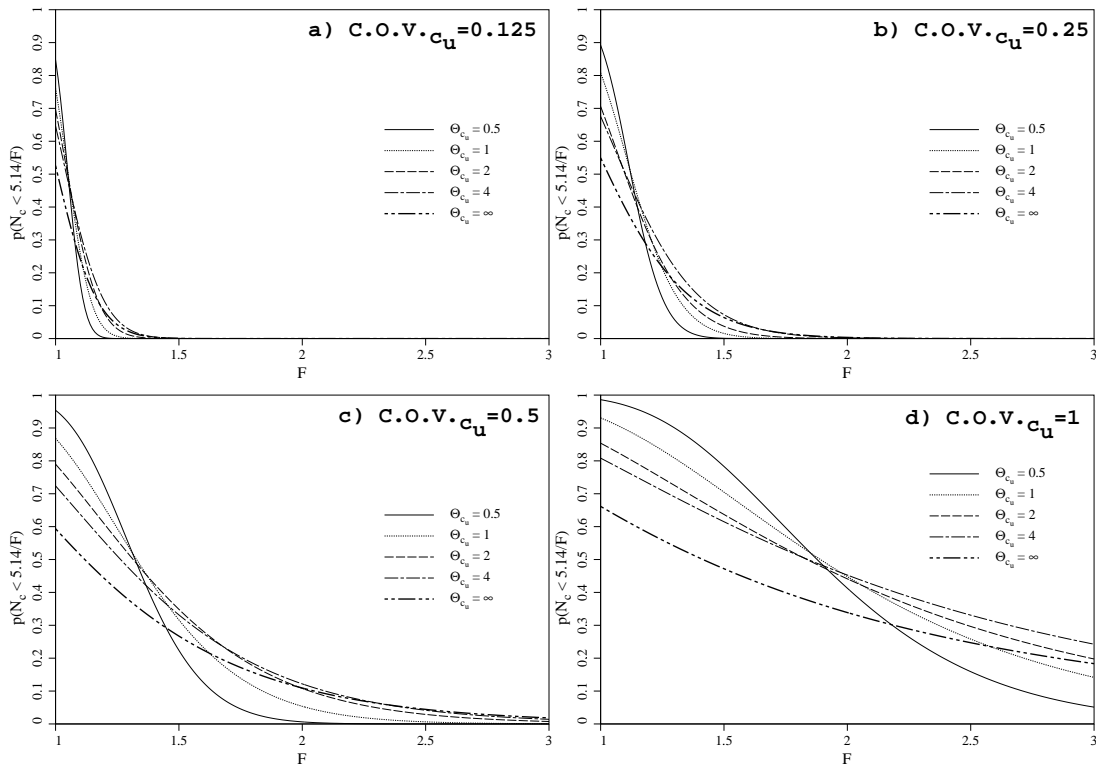
Figure 52. Graphs showing the relationship between $p(N_c < 5.14/F)$ and F for a soil with a) $C.O.V._{c_u} = 0.125$, b) $C.O.V._{c_u} = 0.25$, c) $C.O.V._{c_u} = 0.5$ and d) $C.O.V._{c_u} = 1$.

66

If the goal is to virtually eliminate any possibility of "design failure" involving a bearing capacity calculation based on the mean strength, Figure 52a indicates that for a soil with $C.O.V._{c_u} = 0.125$ (a value at the lower end of the recommended range of Lee et al (1983) and others), a Factor of Safety of $F = 1.5$ would be needed. For an intermediate value of $C.O.V._{c_u} = 0.25$, the required Factor of Safety becomes $F = 2$ (Figure 52b), and for a soil with $C.O.V._{c_u} = 0.5$ (a value at the upper end of the recommended range), the required Factor of Safety increases further to $F = 3$ as shown in Figure 52c. In the case of $C.O.V._{c_u} = 1$ (Figure 52d) – a value that might be considered exceptionally high for most real soils, the need for even higher Factors of Safety is indicated.

An important observation from Figure 52 is that the Correlation Length Θ_{c_u} becomes increasingly relevant to the probabilistic interpretation of the bearing capacity problem as $C.O.V._{c_u}$ gets larger. This is clear from the way the curves are bunched together when $C.O.V._{c_u} = 0.125$ (Figure 52a) while quite divergent when $C.O.V._{c_u} = 1$ (Figure 52d).

In all of Figure 52, the "crossing-over" of the lines corresponding to different Θ_{c_u} values implies that high values of Θ_{c_u} are beneficial to design at low values of F by giving lower probabilities of "design failure", but may be a liability at higher values of F. The explanation lies in the fact that smaller correlation lengths lead to smaller values of $C.O.V._{N_c}$ as shown in Figure 46. Increasing F will therefore result in a steeper fall in the probability of "design failure" as the factored bearing capacity factor rapidly passes through the "bunched up" distribution.

In addition to the expected trend which shows $p(N_c < 5.14/F)$ decreasing as F increases for all Θ_{c_u}, the curves also confirm that a Factor of Safety of 3 is able to reduce the probability of "design failure" to negligible levels for all soils in the recommended range of $0.1 < C.O.V._{c_u} < 0.5$. These results may help explain in a probabilistic context, why Factors of Safety used in bearing capacity calculations are typically much higher than those used in other limit state calculations in geotechnical engineering, e.g. slope stability, earth pressures.

6   Concluding Remarks

This section has shown that soil strength heterogeneity in the form of a spatially varying lognormal distribution can significantly reduce the mean bearing capacity of a strip footing on undrained clay. The following more specific conclusions can be made:

1. As the variance of soil strength increases, the mean bearing capacity decreases. A minimum mean bearing capacity was observed for correlation lengths of approximately one half of the footing width. For still smaller correlation lengths, a modest increase in the mean bearing capacity was detected. It could be speculated that as Θ_{c_u} becomes vanishingly small, the mean bearing capacity factor will continue to increase towards the deterministic Prandtl solution of 5.14. The explanation may lie in the fact that with no spatial correlation, there are no preferred paths of weaker material to attract the mechanism, and the material response is "homogeneous", yielding an essentially deterministic symmetric mechanism at failure.

67

2. The coefficient of variation of the bearing capacity was observed to be positively correlated with both the coefficient of variation of the soil strength and its spatial correlation length.

3. Results have been presented in a probabilistic context, to determine the probability of "design failure", defined as the probability that the actual bearing capacity would be lower than a factored deterministic prediction of bearing capacity using Prandtl's formula based on the mean strength of the soil.

4. By investigating the role of a Factor of Safety applied to the Prandtl solution, it was observed that a value of $F = 3$ would essentially eliminate any possibility of "design failure" for soils with a strength variability within the recommended range.

5. The influence of correlation length on the probabilistic interpretation of the bearing capacity problem was shown to be significant, especially for soils with higher values of $C.O.V._{c_u}$.

7 Acknowledgements

References

L.W. Abramson, T.S. Lee, S. Sharma, and G.M. Boyce. *Slope stability and stabilisation methods.* John Wiley and Sons, 1995.

A. Asaoka and D.A. Grivas. Spatial variability of the undrained strength of clays. *J Geotech Eng, ASCE*, 108(5):743–756, 1982.

A.W. Bishop. The use of the slip circle in the stability analysis of slopes. *Géotechnique*, 5(1):7–17, 1955.

A.W. Bishop and N.R. Morgenstern. Stability coefficients for earth slopes. *Géotechnique*, 10:129–150, 1960.

R.I. Borja, S.R. Lee, and R.B. Seed. Numerical simulation of excavation in elasto-plastic soils. *Int J Numer Anal Methods Geomech*, 13(3):231–249, 1989.

J.D. Brown and G.G. Meyerhof. Experimental study of bearing capacity in layered clays. In *Proc 7th Int Conf Soil Mech Found Eng*, pages 45–51. 1969.

P.T. Brown and J.R. Booker. Finite element analysis of excavation. *Comput Geotech*, 1:207–220, 1985.

S.J. Button. The bearing capacity of footings on a two-layer cohesive sub-soil. In *Proc 3rd Int Conf Soil Mech Found Eng*, pages 332–335. 1953.

A.R. Calderon. The application of back-analysis and numerical modeling to design a large pushback in a deep open pit mine. Master's thesis, Department of Mining Engineering, Colorado School of Mines, 2000.

W.F. Chen. *Limit analysis and soil plasticity.* Elsevier, Amsterdam, 1975.

R.N. Chowdhury. Discussion on stability analysis of embankments and slopes. *J Geotech Eng, ASCE*, 107:691–693, 1981.

R.W. Clough and R.J. Woodward. Analysis of embankment stresses and deformations. *J Soil Mech Found Div, ASCE*, 93:529–549, 1967.

B.F. Cousins. Stability charts for simple earth slopes. *J Geotech Eng, ASCE*, 104(2):267–279, 1978.

G. de Marsily. Spatial variability of properties in porous media: A stochastic approach. In J. Bear and M.Y. Corapcioglu, editors, *Advances in Transport Phenomena in Porous Media*, pages 719–769. NATO Advanced Study Institute on Fundamentals of Transport Phenomena in Porous Media, Dordrecht, Boston, MA, 1985.

D.J. DeGroot and G.B. Baecher. Estimating autocovariance of in-situ soil properties. *J Geotech Eng, ASCE*, 119(1):147–166, 1993.

J.M. Duncan. State of the Art: Limit equilibrium and finite-element analysis of slopes. *J Geotech Geoenv Eng, ASCE*, 122(7):577–596, 1996.

J.M. Duncan. Factors of safety and reliability in geotechnical engineering. *J Geotech Geoenv Eng, ASCE*, 126(4):307–316, 2000.

J.M. Duncan and P. Dunlop. Slopes in stiff fissured clays and soils. *J Soil Mech Found Div, ASCE*, 95(SM5):467–492, 1969.

J.M. Duncan and K.S. Wong. STABR: A computer program for slope stability analysis with circular slip surfaces. Technical report, Virginia Tech, 1985. Department of Civil Engineering.

W. Fellenius. Calculation of the stability of earth dams. In *Proceedings of the 2nd Congress on Large Dams, Washington, D.C.*, volume 4. U.S. Government Printing Office, 1936.

G.A. Fenton. *Simulation and analysis of random fields*. PhD thesis, Department of Civil Engineering and Operations Research, Princeton University, 1990.

G.A. Fenton. Random field modeling of CPT data. *J Geotech Geoenv Eng, ASCE*, 125(6):486–498, 1999.

G.A. Fenton and E.H. Vanmarcke. Simulation of random fields via local average subdivision. *J Eng Mech, ASCE*, 116(8):1733–1749, 1990.

C.M. Goss and D.V. Griffiths. Discussion on rigorous plasticity solutions for the bearing capacity of two-layered clay. *Géotechnique*, 2000. To appear.

D.V. Griffiths. *Finite element analyses of walls, footings and slopes*. PhD thesis, Department of Engineering, University of Manchester, 1980.

D.V. Griffiths. Computation of bearing capacity factors using finite elements. *Géotechnique*, 32(3):195–202, 1982.

D.V. Griffiths. Computation of bearing capacity on layered soils. In Z. Eisenstein, editor, *Proc 4th Int Conf Numer Methods Geomech*, pages 163–170. A.A. Balkema, Rotterdam, 1982.

D.V. Griffiths. Computation of collapse loads in geomechanics by finite elements. *Ing Arch*, 59:237–244, 1989.

D.V. Griffiths. Failure criterion interpretation based on Mohr-Coulomb friction. *J Geotech Eng, ASCE*, 116(GT6):986–999, 1990.

D.V. Griffiths and G.A. Fenton. Three-dimensional seepage through a spatially random soil. *J Geotech Eng, ASCE*, 123(2):153–160, 1997.

D.V. Griffiths and G.A. Fenton. Influence of soil strength spatial variability on the stability of an undrained clay slope by finite elements. In *Slope Stability 2000, Proceeding of GeoDenver 2000*. 2000.

D.V. Griffiths and G.A. Fenton. Bearing capacity of spatially random soil: the undrained clay Prandtl problem revisited. *Géotechnique*, 51(4):351–359, 2001.

D.V. Griffiths and D.J. Kidger. Enhanced visualization of failure mechanisms in finite elements. *Comput Struct*, 56(2):265–269, 1995.

D.V. Griffiths and P.A. Lane. Slope stability analysis by finite elements. *Géotechnique*, 49(3):387–403, 1999.

D.V. Griffiths, F. Molenkamp, and I.M. Smith. Computer implementation of a double hardening model for sand. In P.A. Vermeer and H.J. Luger, editors, *Proc. IUTAM Symp. on Deformation and Failure of Granular Materials*, pages 213–222. A.A. Balkema, Rotterdam, 1982.

M.E. Harr. *Reliability based design in civil engineering*. McGraw Hill, London, New York, 1987.

M.A. Hicks and R Boughrarou. Finite element analysis of the Nelerk underwater berm failures. *Géotechnique*, 48(2):169–185, 1998.

M.A. Hicks and S.W. Wong. Static liquefaction of loose slopes. In G. Swoboda, editor, *Proc 6th Int Conf Numer Methods Geomech*, pages 1361–1368. A.A. Balkema, Rotterdam, 1988.

R.J. Hoeksema and P.K. Kitanidis. Analysis of the spatial structure of properties of selected aquifers. *Water Resour Res*, 21(4):563–572, 1985.

N. Janbu. Slope stability computations. In *Soil Mech. and Found. Engrg. Rep.* Technical University of Norway, Trondheim, Norway, 1968.

F.H. Kulhawy, M.J.S. Roth, and M.D. Grigoriu. Some statistical evaluations of geotechnical properties. In *Proc. ICASP6, 6th Int. Conf. Appl. Stats. Prob. Civ. Eng.* 1991.

T.W. Lambe and F. Silva. The ordinary method of slices revisited. *Geotechnical News*, 13(3):49–53, 1995.

T.W. Lambe and R.V. Whitman. *Soil Mechanics*. John Wiley and Sons, Chichester, New York, 1969.

P.A. Lane and D.V. Griffiths. Asessment of stability of slopes under drawdown conditions. *J Geotech Geoenv Eng, ASCE*, 126(5):443–450, 2000.

J.B. Lechman. The progression of failure in earth slopes by finite element analysis. Master's thesis, Division of Engineering, Colorado School of Mines, 2000.

I.K. Lee, W. White, and O.G. Ingles. *Geotechnical Engineering*. Pitman, London, 1983.

B. Loret and J.H. Prevost. Dynamic strain localisation in fluid–saturated porous media. *J Eng Mech, ASCE*, 117(4):907, 1991.

J. Lowe and L. Karafiath. Stability of earth dams upon drawdown. In *Proc. of the 1st Pan-Am. Conf. on Soil Mech. and Found. Engrg.*, pages 537–552. Mexico, 1960.

T. Matsui and K-C. San. Finite element slope stability analysis by shear strength reduction technique. *Soils Found*, 32(1):59–70, 1992.

R.S. Merifield, S.W. Sloan, and H.S. Yu. Rigorous plasticity solutions for the bearing capacity of two-layered clays. *Géotechnique*, 49(4):471–490, 1999.

F. Molenkamp. Elasto-plastic double hardening model Monot. Technical report, Delft Geotechnics, 1981.

N.R. Morgenstern. Stability charts for earth slopes during rapid drawdown. *Géotechnique*, 13:121–131, 1963.

N.R. Morgenstern and V.E. Price. The analysis of the stability of general slip surfaces. *Géotechnique*, 15(1):79–93, 1965.

D.J. Naylor and G.N. Pande. *Finite elements in geotechnical engineering*. Pineridge Press, Swansea, U.K., 1981.

G.M. Paice. *Finite element analysis of stochastic soils*. PhD thesis, University of Manchester, U.K., 1997.

G.M. Paice and D.V. Griffiths. Reliability of an undrained clay slope formed from spatially random soil. In J-X. Yuan, editor, *IACMAG 97*, pages 1205–1209. A.A. Balkema, Rotterdam, 1997.

P. Perzyna. Fundamental problems in viscoplasticity. *Advances in Applied Mechanics*, 9:243–377, 1966.

D.M. Potts, G.T. Dounias, and P.R. Vaughan. Finite element analysis of progressive failure of Carsington embankment. *Géotechnique*, 40(1):79–102, 1990.

S. Sarma. Stability analysis of embankments and slopes. *J Geotech Eng, ASCE*, 105:1511–1524, 1979.

I.M. Smith and D.V. Griffiths. *Programming the Finite Element Method*. John Wiley and Sons, Chichester, New York, 3rd edition, 1998.

I.M. Smith and D.K.H. Ho. Influence of construction technique on performance of braced excavation in marine clay. *Int J Numer Anal Methods Geomech*, 16, 1992.

I.M. Smith and R. Hobbs. Finite element analysis of centrifuged and built-up slopes. *Géotechnique*, 24(4):531–559, 1974.

N. Snitbhan and W.F. Chen. Elastic-plastic large deformation analysis of soil slopes. *Comput Struct*, 9:567–577, 1976.

E. Spencer. A method of analysis of the stability of embankments assuming parallel interslice forces. *Géotechnique*, 17(1):11–26, 1967.

E.A. Sudicky. A natural gradient experiment on solute transport in a sand aquifer: Spatial variability of hydraulic conductivity and its role in the dispersion process. *Water Resour Res*, 22(13):2069–2083, 1986.

D.W. Taylor. Stability of earth slopes. *J. Boston Soc. Civ. Eng.*, 24:197–246, 1937.

K. Terzaghi and R.B. Peck. *Soil Mechanics in Engineering Practice*, page 237. John Wiley and Sons, New York, 1967.

R. Torres and T. Coffman. Liquefaction analysis for CAS: Willow Creek Dam. Technical Report WL-8312-2, U.S. Department of the Interior, Bureau of Reclamation, 1997.

E.H. Vanmarcke. *Random fields: Analysis and synthesis*. The MIT Press, Cambridge, Mass., 1984.

R.V. Whitman and W.A. Bailey. Use of computers for slope stability analysis. *J Soil Mech Found Div, ASCE*, 93(SM4):475–498, 1967.

F. S. Wong. Uncertainties in FE modeling of slope stability. *Comput Struct*, 19:777–791, 1984.

P.K. Woodward and D.V. Griffiths. Observations on the computation of the bearing capacity factor N_γ by finite elements. *Géotechnique*, 48(1):137–141, 1998.

O.C. Zienkiewicz and I.C. Cormeau. Viscoplasticity, plasticity and creep in elastic solids. a unified approach. *Int J Numer Methods Eng*, 8:821–845, 1974.

O.C. Zienkiewicz, M. Huang, and M. Pastor. Localization problems in plasticity using finite elements with adaptive remeshing. *Int J Numer Anal Methods Geomech*, 19(2):127–148, 1995.

O.C. Zienkiewicz, C. Humpheson, and R.W. Lewis. Associated and non-associated viscoplasticity and plasticity in soil mechanics. *Géotechnique*, 25:671–689, 1975.

O.C. Zienkiewicz and R.L. Taylor. *The Finite Element Method*, volume 1. McGraw Hill, London, New York, 4th edition, 1989.